UNIVERSIDADE ESTADUAL DE LONDRINA

ANDINA ALAY LERMA

MODELLING P-SV SEISMIC WAVE PROPAGATION FOR BRAZILIAN TERRITORY IN HOMOGENEOUS MEDIA

Londrina
2021

ANDINA ALAY LERMA

MODELLING P-SV SEISMIC WAVE PROPAGATION FOR BRAZILIAN TERRITORY IN HOMOGENEOUS MEDIA

Masters dissertation presented to the Department of Mathematics at the State University of Londrina, as a partial requirement to obtain the MASTER's Degree in Applied and Computational Mathematics.

Advisor: Prof. Dr. Paulo Laerte Natti

Londrina
2021

Cataloging prepared by the Technical Processes Division of the Central Library of the State University of Londrina
International Data of Cataloging-in-Publication (CIP)

L616m Alay Lerma, Andina.
Modelling P-SV Seismic Wave Propagation for Brazilian Territory in Homogeneous Media /
Andina Alay Lerma. – Londrina, 2021.
66s. : il.

Advisor: Paulo Laerte Natti.
Co-advisor: Eliandro Rodrigues Cirilo.
Co-advisor: Neyva Maria Lopes Romeiro.
Dissertation(Master in Applied and Computational Mathematics)- State University of Londrina, Exact Sciences Center, Graduate Program in Applied and Computational Mathematics, 2021.

Includes Bibliography.

1. Seismic Waves -Thesis. 2.Mathematical Modeling -Thesis. 3.Finite Difference Method -Thesis. 4.Numerical Simulations. -Thesis. I. Laerte Natti, Paulo. II. Rodrigues Cirilo, Eliandro. III. Lopes Romeiro, Neyva Maria. IV. State University of Londrina. Exact Sciences Center. Graduate Program in Applied and Computational Mathematics. V. Title.

CDU 51

Catalogação elaborada pela Divisão de Processos Técnicos da Biblioteca Central da Universidade Estadual de Londrina
Dados Internacionais de Catalogação -na-Publicação (CIP)

L616m Alay Lerma, Andina.
Modelagem da Propagação das Ondas Sísmicas P-SV para o Território Brasileiro num Meio Homogéneo. /
Andina Alay Lerma. - Londrina, 2021.
66f. : il.

Orientador: Paulo Laerte Natti.
Coorientador: Eliandro Rodrigues Cirilo.
Coorientador: Neyva Maria Lopes Romeiro.
Dissertação (Mestrado em Matemática Aplicada e Computacional)- Universidade Estadual de Londrina, Centro de Ciências Exatas, Programa de Pós-Graduação em Matemática Aplicada e Computacional, 2021.

Inclui Bibliografia.

1. Ondas Sísmicas. -Tese. 2.Modelagem Matemática. -Tese. 3.Método das Diferenças Finitas. -Tese. 4. Simulações Numéricas. -Tese. I. Laerte Natti, Paulo. II. Rodrigues Cirilo, Eliandro. III. Lopes Romeiro, Neyva Maria IV. Universidade Estadual de Londrina. Centro de Ciências Exatas. Programa de Pós-Graduação em Matemática Aplicada e Computacional. V. Título.

CDU 51

ANDINA ALAY LERMA

MODELLING P-SV SEISMIC WAVE PROPAGATION FOR BRAZILIAN TERRITORY IN HOMOGENEUS MEDIA

Masters dissertation presented to the Department of Mathematics at the State University of Londrina, as a partial requirement to obtain the MASTER's Degree in Applied and Computational Mathematics.

EXAMINATION BOARD

Prof. Dr. Paulo Laerte Natti
Londrina State University, UEL

Prof. Dr. Adeval Lino Ferreira
Maringá State University, UEM

Prof. Dra. Poliane Cristina de Farias
Londrina State University, UEL

Londrina, July, 28, 2021.

ACKNOWLEDGMENT

CAPES - Coordination for the Improvement of Higher Education Personnel) - for the financial support given for the development of this work.

To my advisor Dr. Paulo Laerte Natti, for all the dedication, competence and patience.

To my teachers, Dr. Eliandro Rodrigues Cirilo e Dr. Neyva Maria Lopes Romeiro.

To my family for their unconditional support.

To my friends for motivating me to improve.

ALAY, Andina Lerma. **Modelling P-SV Seismic Wave Propagation for Brazilian Territory in Homogeneous Media:**. 2021. Dissertation (Master in Applied and Computational Mathematics.) – State University of Londrina, Londrina, 2021.

ABSTRACT

In the literature, there are few works of seismic modelling in Brazil. We know that Brazil is in the central part of the South American plate making the country have many seismic, mostly low intensity. However, some known faults have already generated intense earthquakes in the Brazilian territory. Earthquakes are vibratory phenomena of short duration and, at times, of great intensity. They are generated around a source called hypocenter, where large displacements of masses are produced, generating longitudinal and transverse waves. The longitudinal waves vibrate in the direction of the wave propagation and they are the first to be observed. The transverse waves vibrate perpendicular to the propagation direction and they delay in relation to longitudinal waves. In this context, the mathematical modelling of seismic waves allows the elaboration of theoretical seismograms that make it possible to predict the characteristics of earthquakes, depending on the local geological conditions. This work modelling the propagation of P(longitudinal waves) and SV (transverse waves) seismic waves by equations of motion in elastic media, since the Earth behaves as a deformable material. So, our partial differential equations (PDE) describe the propagation of seismic waves in a vertical two-dimensional system (x and z coordinates), given a source, and initial and boundary conditions. The vertical two-dimensional domain is considered rectangular. The source is modeled by a Gaussian pulse function, located at a point inside the domain. To solve this PDE system, the finite difference method (FDM) is used. The computational algorithm was developed. Numerical simulations were performed in a homogeneous medium using OCTAVE.

Key Words: Seismic Waves. Mathematical Modelling. Finite Difference Method. Numerical Simulations. Seismogram.

ALAY, Andina Lerma. **Modelagem da Propagação das Ondas Sísmicas P e SV para o Território Brasileiro num Meio Homogêneo.** 2021. Dissertação (Mestrado em Matemática Aplicada e Computacional) – Universidade Estadual de Londrina, Londrina, 2021.

RESUMO

Na literatura existem poucos trabalhos de modelagem sísmica no Brasil. Sabemos que o Brasil está na parte central da placa sul-americana fazendo com que o país tenha muitos sismos, a maioria de baixa intensidade. No entanto, algumas falhas conhecidas já geraram terremotos intensos no território brasileiro. Os terremotos são fenômenos vibratórios, de curta duração e, às vezes, de grande intensidade. São gerados em torno de uma fonte denominada hipocentro, onde são produzidos grandes deslocamentos de massas, gerando ondas longitudinais e transversais. As ondas longitudinais vibram na direção da propagação das ondas e são as primeiras a serem observadas. As ondas transversais vibram perpendicularmente à direção de propagação e atrasam em relação às ondas longitudinais. Nesse contexto, a modelagem matemática de ondas sísmicas permite a elaboração de sismogramas teóricos que possibilitam prever as características dos terremotos, dependendo das condições geológicas locais. Este trabalho modelou a propagação das ondas sísmicas P (ondas longitudinais) e SV (ondas transversais) por meio de equações de movimento em meios elásticos, uma vez que a Terra se comporta como um material deformável. Portanto, essas equações diferenciais parciais (PDE) descrevem a propagação de ondas sísmicas em um sistema bidimensional vertical (coordenadas x e z), dada uma fonte e condições iniciais e de contorno. O domínio bidimensional vertical é considerado retangular. A fonte é modelada por uma função de pulso gaussiana, localizada em um ponto dentro do domínio. Para resolver este sistema PDE, o método das diferenças finitas (FDM) é usado. O algoritmo computacional foi desenvolvido. As simulações numéricas foram realizadas em meio homogêneo usando OCTAVE.

Keywords: Ondas Sísmicas. Modelagem Matemática. Método das Diferenças Finitas. Simulações Numéricas. Sismograma.

SUMMARY

Contents

LIST OF FIGURES

LIST OF TABLES

LIST OF MATHEMATICAL SYMBOLS

F_i = Components of the applied force on an infinitesimal cube.

$\tau_{i,j}$ = Tensor stress

x_j = Spatial component

f_i = Force density component

m = Mass

ρ = Density

u_i = Components of the displacement vector

γ_i = Attenuation constants

$\delta_{i,j}$ = Kronecker Delta

$\lambda,\ \mu$ = Lame parameters

$E_x,\ E_z$ = Body force

c = Gaussian source width, in time

a = Source amplitude

κ = Gaussian source width, in space

$u_x{}^{l}_{i,k},\ u_z{}^{l}_{i,k}$ = Discretization of components of displacement vector

$AP1,\ AP2,\ AE1,\ AE2,\ AN1$ and $AN2$ = Discretization constants

LIST OF ABREVIATIONS

FDM = Finite Difference Method

LR = Rayleigh waves

LQ = Love waves

PDE = Partial Differential Equations

P = Pressure or longitudinal wave

S = Transversal wave

SH = S-wave horizontal movement, perpendicular to the direction of wave motion.

SV = S-wave vertical movement, perpendicular to the direction of wave motion.

SFDM = Staggered Finite Difference Method

1 INTRODUCTION

Earthquakes are vibratory movements caused by the internal crumbling of the earth's crust and propagate in all directions in the form of seismic waves, which reach the surface. They can be caused by the movement of tectonic faults,volcanic explosions, landslides and human activities, such as hydroelectric reservoirs, which, due to the accumulation of water, presses the lower layers of the terrain, which can generate ruptures and, consequently, earthquakes (ASSUMPÇÃO; NETO, 2000). Seismic waves can be P (primary) waves that are the first to reach the surface. In the case of S (secondary) waves, the particles move in the direction perpendicular to the propagation path, generating SV waves (movement of the particles is totally vertical) and SH (movement that occurs in the horizontal plane), inducing shear deformations. The displacement of these waves, when represented in seismograms, it is possible to know the magnitude of these seismic events, due to the amplitude with which they occur in time. The Richter scale is used to measure the power of earthquakes, using a logarithmic scale for certain frequencies. In Brazil, earthquakes are shallow and moderate in intensity, but they can cause material damage and economic loss. Since the earthquakes are natural disasters, against which there is no defense or protection, it is important to mitigate damage in this type of phenomenon. It is necessary to carry out studies of prevention, risk and seismic prediction, using data from the World-Wide Standard Seismograph Network and theoretical work. The use of theoretical-computational methods allows us to predict and minimize the effects of a variety of earthquakes.

The numerical solution of the system of of differential equations that model the seismic waves P, SV and SH is obtained by several methodologies. In this work we use the Finite Difference Method (FDM) due to its easy. Historically, the first works on seismic wave propagation used this method to find numerical solutions (ALTERMAN, KARAL, 1968; VIREUX, 1986). More recently, Zhang et al. (2006) calculated high-order non-staggered finite difference scheme for seismic waves. Fernandes et al. (2009) used FDM to obtain the P and S wavefield through the acoustic wave. In (SILVA et al., 2009), the authors parallelized the algorithm to obtain the solutions of seismic wave using finite differences time-domain. Virieux et al. (2012) used two techniques for solving the elastodynamic equations, one of which was the FDM. In 2012, Contreras et al., solved the velocity stress and displacement stress equations by FDM. In 2013, Bai et al. made an comparison of the two types of approaches for the seismic phenomenon, in both cases the Staggered Finite Difference Method (SFDM) was used, but with different order of precision. Zhang et al. (2013) used the FDM for P and S wavefield simulations for first and second order separated wave equations. In 2014, Alcrudo used the software Sofi2D to solve the elastic and viscoelastic wave equations numerically by the FDM. Lisitsa et al. (2016) developed a hybrid algorithm, using FDM technique to simulate seismic waves. Takenaka et al. (2017) solved the subglobal model, using the elastic wave equations in quasi-Cartesian coordinates, by means of the SFDM. In 2019, Ren at al. proposed an implicit Staggered-coordinates, using Finite Difference scheme for seismic waves.

About modeling the physical and mathematical domains of the earthquake depend on the region where it occurs and sometimes it is necessary to consider the curvature of the Earth. For the computational mesh, different geometries are used for the discretization of the domain, according to the topography of the region to be studied. On the other hand, for near-surface earthquakes, called local earthquakes, it is possible to have a homogeneous rectangular domain. In the case of deep earthquakes, the use of non-Cartesian coordinates is necessary. In this context of mathematical modelling of domains to describe earthquakes, Alterman and Karal (1968) used semi-infinite region, like a rod. Zhang et al. (2006,2013) used a grid defined by a curvilinear coordinate system. In 2012, Virieux et al. used a large-scale modelling for an irregular complex topography. Lisitsa et al. (2016) introduced part of the complexity of the topography, close to the free surface, in the simulations. In (TAKENAKA et al., 2017) was used a three-dimensional model with a spherical polar coordinate grid. In 2019, Ren et al. used 2-D and 3-D domain for propagation of seismic waves.

On the medium where the waves are transmitted, it can be isotropic or anisotropic. Most of the works use homogeneous layers, using different elastic constants for each of the media separated by interfaces. The phenomenons generated by the interaction of seismic waves with interfaces are refractions, diffractions and reflections (ROSA FILHO et al., 2003). In (PEKERIS et al., 1965), the different medias were described by different Lame's constants and velocities. Alterman and Karal (1968) used layered interfaces to show the variation of the surface waves according to the depth and density functions. Virieux (1986) represented the interface by changes on density and elastic parameters. Vashisth and Gogna (1993) used the wave propagation in porous solid media and in isotropic impermeable elastic solid. In 2009, Fernandes et al. used irregular interfaces getting reflections, and diffractions in each media, given by different physical properties. Silva et al. (2009) works with different solid media, while Contreras et al. (2012) used solid-fluid media. In (BAI et al., 2013) modeled the interface by an implicit condition. Zhang et al. (2013) used shallow and low velocity regions. Alcrudo (2014) used an interface given by the physical properties of the medium.

Regarding the mathematical modeling of earthquakes, there are several approaches. Normally, the initial conditions are considered to be in a state of quiescence throughout the domain, including the borders. This state of quiescence is altered by an initial force known as hypocenter. The waves generated by the source must reach the edges and pass through, free conditions, so that no artificial reflections occur, which would affect the modeling of the seismic wave propagation. In (ALTERMAN, KARAL, 1968), the boundary conditions for stress and displacement at the surface are zero, while at the interface they are continuous. Virieux (1986) used free boundary conditions, however the interface is represented by changes in the Lame parameters. Fernandes et al. (2009) used the Clayton boundary conditions. Contreras et al. (2012) used boundary conditions at the fluid-solid interface, where the displacements and normal stresses are continuous. Bai et al. (2013) used attenuating boundary conditions. Hustedt et al. (2004) used the Perfectly Matched Layer (PML), absorbing boundary condition, which were also used in the works like (VIRIEUX et al., 2012; ZHANG et al., 2013; TAKENAKA et al., 2017;

BENITO et al., 2017).

In this context, our work describes the P and SV seismic waves to the Brazilian territory. According to the data, earthquakes in Brazil occur, on average, at depths less than 50km. To model the propagation of the P-SV waves, we solve a system of partial differential equations (PDE) with attenuation terms. For the resolution of this system of equations, the FDM is used. The discretization of the computational model was realised in rectangular coordenates, because the source of the earthquakes are very close to the surface, compared to the radius of the earth. The boundary conditions are also discretized by FDM.

The work has the following structure. Chapter 2 presents the characteristics of seismic waves, the Earth's interior structure, its tectonic plates and where earthquakes occur most frequently. In chapter 3 we developed the mathematical modeling of the partial differential equations, and the initial and boundary conditions, to solve our problem. Initially, we present a short bibliographic review of the models already used to describe the propagation of P and S waves. Then, the seismic wave model is developed in homogeneous environments. Finally, the domain, and the initial and contour conditions are chosen. In chapter 4 the discretization of the model in a rectangular domain is developed by FDM. Then a consistency analysis of the discretized model is performed. In Chapter 5 the numerical simulations are carried out and then the results are analyzed.

2 SISMICITY

In this chapter, some basic definitions for the understanding of seismic phenomenon are presented. Firstly, the internal structure of the Earth is presented, which is given by different layers, each one with different properties, which affect the behavior of seismic waves. In the second part, tectonic plates are described and how and where movements occur due to the interaction between then, movements that can be of various types, causing changes in the Earth's geography known as earthquakes that are more likely in some continents. The third part describes the seismic hazard around the world, as well as the countries in which earthquakes are most frequent. So, because it is a study on the South American plate , where intense earthquake cases also occur, the level of risk for the countries is presented. In the special case of Brazil, it is affected by earthquakes caused by the tensions within the South American plate, and the faults and seismic risk zones are also shown. Finally, the types of seismic waves are defined.

2.1 EARTH'S INTERNAL STRUCTURE

There are two ways to define the structure of the earth, physically and chemically. In the chemical way, it is separated as follows: Crust, it is the most superficial layer which is habitable, and its thickness is between 11km in the ocean ridges and 40 km up to 70 km in the Andes and the Himalayas. Mantle, it is the deepest layer of land, with 2,850 km thick. The border between the mantle and the crust is called the Mohorovic discontinuity. This discontinuity is marked by the difference in density of the rocks, which increases the speed of the seismic waves. Core, it is formed by sub-layers, the first solid known as inner core of 1,270 km thick, and the second semi-solid or outer core of 2,200 km thick. The border between the mantle and the core is marked by the Gutenburg discontinuity that shows the most noticeable difference in density, where some seismic waves slow down and others disappear.

The structure of the earth can also be physically divided as follows: Lithosphere is formed by the Earth's crust and a part of the mantle; it is relatively cold, it behaves like a solid rigid, and it is in this layer the tectonic plates are located. Asthenosphere, it is between 30 km to 130 km thick. It is formed by a part of the mantle and is located below the Lithosphere. It is a layer of the Earth, where seismic waves reduces their speed due to the composition malleable silicate materials, in solid state and partially or totally melted. It is also the region where the movement of tectonic plates occurs because the state of the material is viscous, with solid and liquid behavior, where tectonic plates float. Mesospheric, it has 660 km thick, and it formed by the solid part of the Mantle. It is located below the Asthenosphere, and it is characterized by the strong increase in the speed of seismic waves due to the high density of iron and magnesium minerals. The outer core of 2,200 km thick and inner core of 1,270 km thick are the innermost geologic layer of the Earth. Figure 2.6 shows the layers of the Earth.

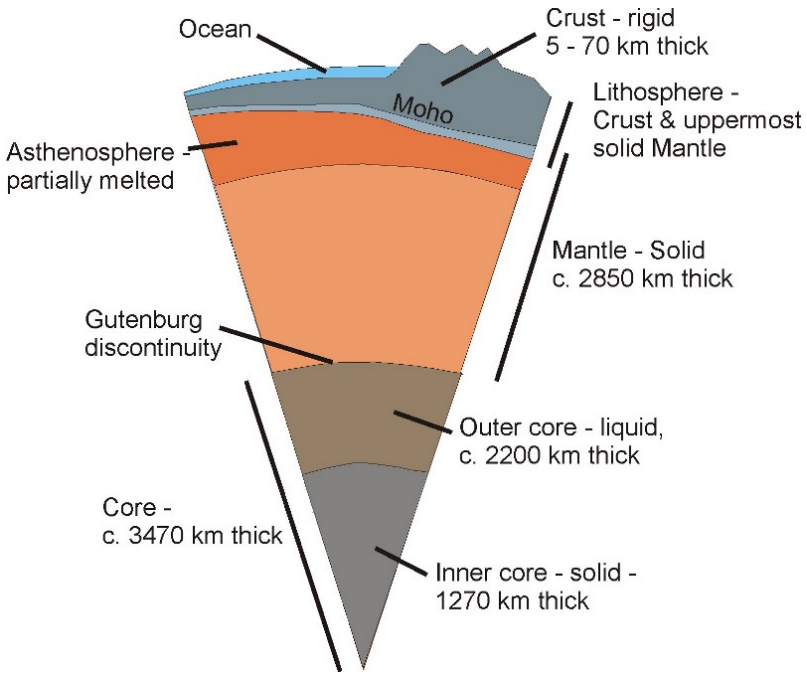

Figure 2.1: The internal structure of the Earth
Source: Geological Survey Ireland (SLEEMAN et al., 2004)

2.2 TECTONIC PLATES

The Earth's outer layer is formed by tectonic plates that make up the crust and mantle. These plates move, due to the convection currents of the Earth's internal regions. The Isostacia phenomenon allows the gravitational equilibrium compensation of these movements, this explains that the densest rocks descend while the tectonic plates float. The plates are not stable, so they interact with each other, and that occurs at their edges where the plates are pushed together, pulled apart, and where plates slide laterally past each other. To this is added that the plates can be oceanic and continental, the contact between this type of plates causes phenomena with different characteristics for each region where it occurs. The collision of the oceanic-continent plates causes the formation of subduction zones, which produces the lifting of land, such as the Andes mountain range. The collision of the ocean-ocean plates also creates a subduction zone that forms arcs of islands. The continent-continent plate collision causes an elevation of the terrain, as in the case of the Himalayas (GATES et al., 2006).

According to the type of interaction of the lithosphere and the asthenosphere, the movement of the tectonic plates at their borders causes the faults close to them to be activated. These areas have the potential for earthquakes to occur. In tectonic movement, it is possible to classify three types of interaction between the borders of the plates: spacing, collision and, sliding between one plate and another, this is shown in Figure 2.2. Where the diverging fault is known to be constructive, due to the material that is generated when the plates are separated. In convergent faults also known as destructive, since great material in the oceanic crust is destroyed by the subduction movement in the earth's crust. If the movement occurs by continental plates and these collide, they generate rock uplift. Finally, the transforming faults retain their edges, because their movement is right and left lateral-slip (GATES et al., 2006).

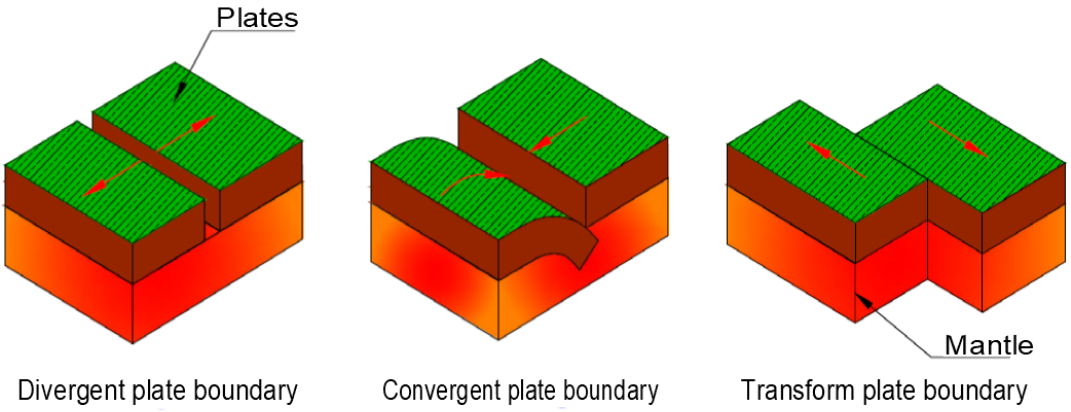

Figure 2.2: Three types of tectonic movement. First figure: The borders of the plates are spacing, Second figure: The borders of the plates are collision. Third figure: The borders of the plates are sliding between plates

Source: Adapted from (GARCIA et al., 2018)

In the Figure 2.3, we see the main tectonic plates, given by their dimensions, namely: the Pacific Plate, which is the largest of the plates, it is below the Pacific Ocean. The second largest plate is the North American Plate, which has an oceanic part and a continental part. The Eurasian Plate contains the European and Asian continents, which forms a zone of volcanic eruptions on its borders with the North American plate. The African plate covers the African continent and also has an oceanic part. All the limits of the African plate are very divergent, except the one that has with the Eurasian plate. The Antarctic plate contains this continent and the surrounding oceans. The Indo-Australian Plate was generated by the fusion of two plates, and it covers the Indian continent, the East of the Indian Ocean, Australia, Melanesia and extending to New Zealand. Finally, the South American plate covers the American continent and a part of the Atlantic ocean. There are also plates that are smaller in size than those mentioned above, which are located between the larger plates, which are known as secondary plates, they are: Somali, Nazca, Amurian, Sunda, Philippine, Okhotsk, Arabian, Yangtze, Caribbean, Cocos, Caroline, Scotia, Juan de Fuca, Burma and New Hebrides. The South American plate has a border in the west with the Nazca and Antarctica plates, in the east with the Africa Plate and in the north with the Caribbean plate.

2.3 Seismic magnitude scales

The magnitude of a seismic event can be measured on scales, which are obtained by seismograms. In 1935 Charles F. Richter, based on the record of amplitudes given by seismographic stations, expressed these in logarithmic scale. The increace of a point implies 10 times the amplitude of the wave, so that on this scale there are no lower or upper limits. However, these limits are given by the mechanics of the rocks. The Richter scale is limited for certain wave frequencies and distance, being created new scales based on it, for different types of oscillations. These scales are: Seismic Moment magnitude (Mw), Energy magnitude (Mk), Surface-wave magnitude (Ms), Body-wave magnitude (Mb) and Local magnitude Richter (ML).

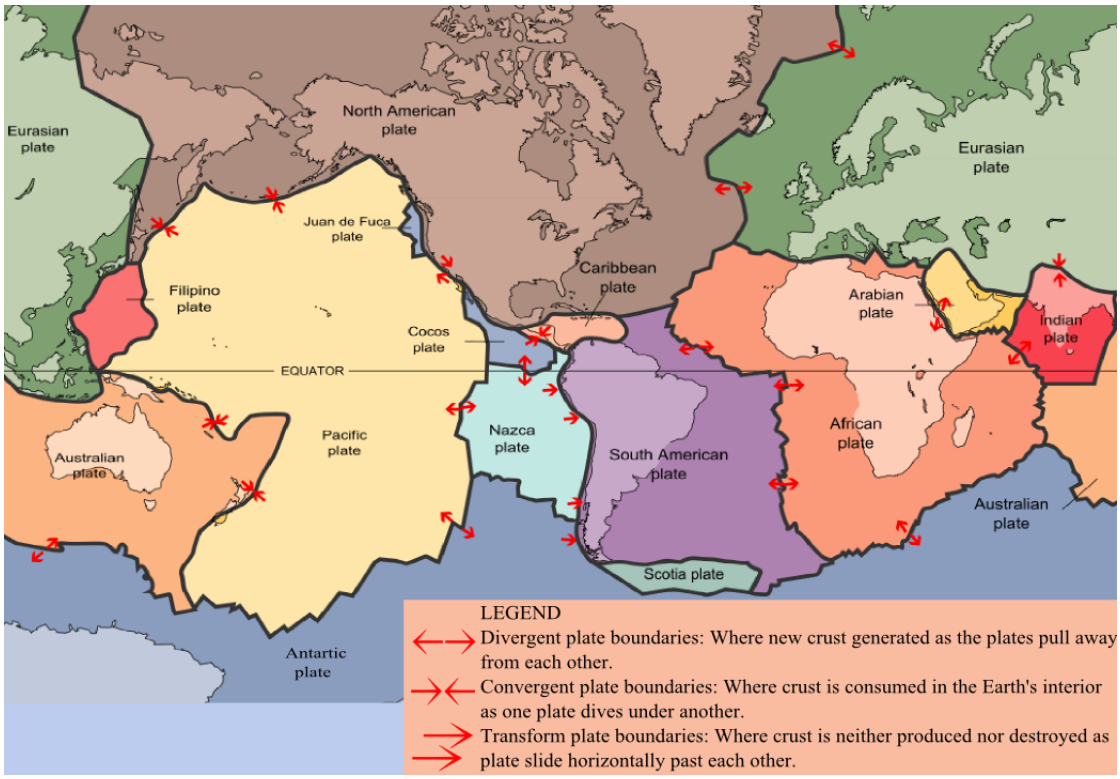

Figure 2.3: Types of interactions between major tectonic plates around the World
Source: Adapted from (KIOUS et al., 1996)

Each of these scales mentioned is equivalent to some extension to the Richter scale, but for different conditions in which an earthquake occurs. Among these scales, the scale (Ms) can be used for earthquakes with a depth of less than 50 km, because they generate detectable surface waves.

$$Ms = \log_{10}(As/T) + 1.66\log_{10}(\Delta^{\circ}) + 3.3 \tag{2.1}$$

where As is the amplitude of the surface wave (μm), T is the wave period ($18s$-$22s$), Δ is the epicentral distance, in degrees (BÅTH, 1966). To measure the magnitudes of the P waves, Gutenberg (1945) proposed the following equation:

$$Mb = \log_{10}(Ap/T) + 0.01\log_{10}(\Delta^{\circ}) + 5.9 \tag{2.2}$$

where Ap is the maximum amplitude of the ground movement, T is the wave period ($1s$-$5s$).

In the case of moderate earthquakes, the surface waves are hardly detectable, so the scale (Mr) is used, as for example in the Brazilian lithosphere. It can also be said that the Regional scale (Mr) is equivalent to (Mb) elaborated for attenuation conditions (ASSUMPÇÃO; NETO, 2000). The formula to obtain the magnitude on the scale (Mr) is:

$$Mr = \log_{10}(V) + 2,3\log_{10}(R) - 2,48 \tag{2.3}$$

where V is the velocity of the P wave $(\mu m/s)$ ($V = 2\pi A/T$,A = amplitude, T = period) and R is the epicentral distance (km).

2.4 SEISMIC INTENSITY SCALES

The seismic intensity is a qualitative measure that allows knowing the effects produced in a specific place, such as buildings, objects, people and the environment.

Mercalli Scale

This scale is known as the Modified Mercalli scale (MM), it allows seismologists to know the effects through 12 degrees that describe the effects on the surface, where the earthquake occurred. This scale does not give a relationship to the magnitude of the earthquake.

Peak ground acceleration (PGA)

It is a very useful measure in the field of Engineering that establishes seismic risk zones and seismic norms. This measures the alterations experienced by the ground surface, which is related to the intensity of the earthquake. The acceleration used is the intensity of the gravitational field, represented as g, expressed in N/kg.

In Table 2.1 shows the descriptions for each degree of intensity on the Mercalli scale, related to Peak ground accelaration.

2.5 EARTHQUAKES AROUND THE WORLD

The earth as a whole is dynamic, and one of the main phenomena caused by this dynamic is earthquakes. The vast majority of these earthquakes are produced at the borders of tectonic plates. In these places; are also the largest number of volcanoes due to the subduction of the plates, such as the chain of volcanoes known as the Pacific Ring of Fire. The great energy released due to the movement in the rupture zones generate the most intense earthquakes; and when these forces move the plates, it causes other faults, which are activated due to the compression and deformation movements. Note that this accumulation of energy generates earthquakes far from the edges of the plate (ERICKSON, 2014).

The places with the highest seismicity are located in the Ring of Fire of the Pacific Ocean, where countries as Japan are historically affected by the effects of recurrent earthquakes. Other regions of the Earth also have a lot of seismic activity , as in Italy, in the southern zone, where the Eurasian and African plates collide. This is also where the most active volcanoes are located, such as Etna, Stromboli and Vesuvius. The western region of the United States is located between the North American and Pacific plates, where the San Andrés Fault extends throughout California. The Turkey is located between the Eurasian and Arabian plates where, the region has intense earthquakes in the region known as Anatolian Faults. Also in Iran, due to the shock of these plates, many seismic zones occur. In Indonesia there are numerous surface and underwater volcanic eruptions. The China is located within the Eurasian tectonic plates, and the the most frequent earthquakes occur in the southwestern area.

Earthquakes are considered one of the most destructive phenomena that change the

Intensity	Description Damage	PGA(g)
I	It is not felt, slight effects in the environment except under favorable special conditions	
II	Felt by few people standing on upper floors of buildings, some slight objects can be moved.	< 0.003
III	Felt by persons indoors especially on upper floors of buildings.	$0.004 - 0.008$
IV	Slight objects oscillate, similar to the movement produced by a passing truck.	$0.008 - 0.015$
V	Felt outdoors by few persons. The house doors swing, and some light objects in bad position are broken.	$0.015 - 0.04$
VI	Felt by all people and objects. Badly designed structures Buildings crack or fall.	$0.04 - 0.08$
VII	People cannot stand upright, objects vibrate or break. Damage slight in designed structures and considerable damage in poorly built. Some landslides occur in sandy ravines.	$0.08 - 0.15$
VIII	Considerable damage in ordinary buildings with partial collapse. Damage great in poorly built structures. Fall of columns, monuments, walls and slight cracking of streets.	$0.15 - 0.30$
IX	General panic. Damage great in ordinary buildings. Damage partial in designed structures. Crack of streets and damaged underground pipes.	$0.30 - 0.60$
X	Well-designed frame structures thrown out of plumb. Large landslides.	$0.60 - 1.0$
XI	Few structures remain standing. Underground pipes completely destroyed. Bridges destroyed.	$\sim 1 - 2$
XII	Total destruction of structures. Damage total. Objects thrown into the air.	~ 2

Table 2.1: Relation between the degree of intensity on the Mercalli scale and Peak ground accelaration. Adapted from (ASSUMPÇÃO; NETO, 2000)

geography of territory in a short period of time. Countries mentioned above have to deal with it frequently, resulting in human and economic loss. In order to make decisions that help mitigate the damage caused by earthquakes, seismic hazard was analyzed throughout the planet. In Figure 2.4, it is observed that the colors represent the level of seismic risk in those places. White and green colors represent low hazard; yellow and orange a moderate hazard. Black and pink colors represent high seismic hazard; red and brown indicate a very high seismic hazard. It is observed that most of the planet (70 %) has a low level of seismic hazard, while moderate level (22 %), (6 %) high hazard level and (2 %) have a very high seismic hazard (SHEDLOCK et al., 2000). These risk level values are given as a function of gravity g.

2.5.1 Earthquakes in South America

As seen in Figure 2.4, the west of South American continent has a very high seismic hazard. The South American plate that contains the continent is in contact with the plates of the Caribbean, Nazca and Antarctica, being with these a dynamic place, with zones of tectonic subduction

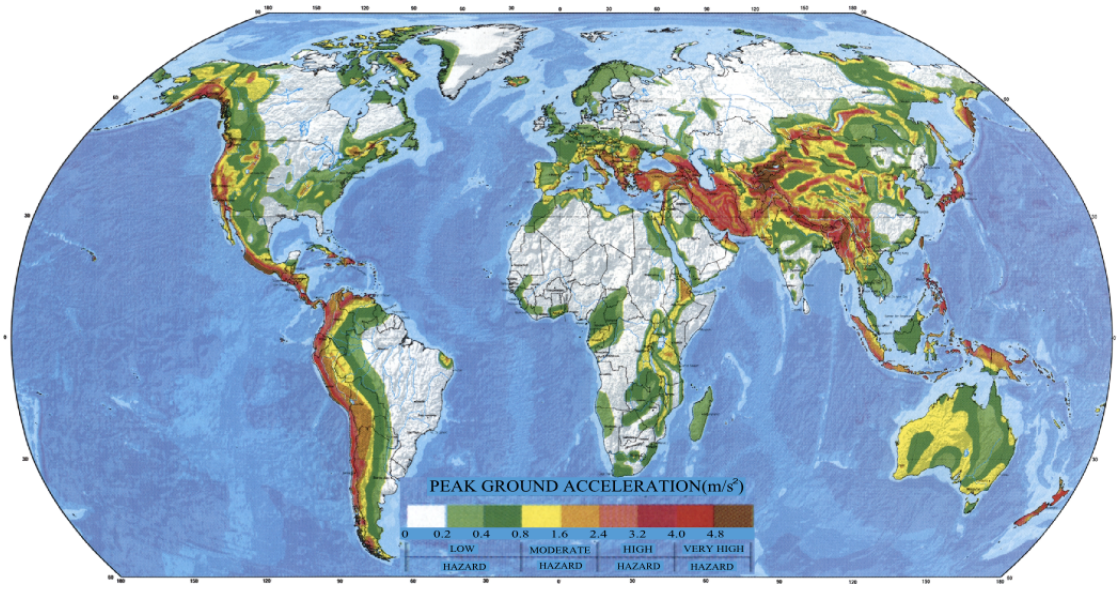

Figure 2.4: The Global Seismic Hazard Map. White and green correspond to low seismic hazard (O%-8%g), yellow and orange correspond to moderate seismic hazard (8%-24%g), pink and dark pink correspond to high seismic hazard (24%-40%g), and red and brown correspond to very high seismic hazard (greater than 40% g)
Source: Adapted from (SHEDLOCK et al., 2000)

and tectonic transformation faults.

The countries that are relatively stable, because they are within the South American and Patagonian platform, are: the entire Brazilian territory, Paraguay, Uruguay, Guyana and Suriname, as well as the central and southern regions of Venezuela, eastern Colombia, Ecuador, Peru, Bolivia and most of the Argentine territory. The other regions are seismically active. They are formed by the chain of mountains of the Andes along the entire western margin of the continent, which connects with the mountainous zone of the Caribbean, forming the contact border of the South American Plate with the Caribbean, Nazca, and Antarctica plates, which is most of the territories of Venezuela, Colombia, Ecuador, Peru and Chile, the Altiplanica region of Bolivia and the western sector of Argentina (AMÉRICA et al., 1997). Figure 2.5 shows the areas with the highest number of earthquakes, as well as their intensity represented in colors.

2.5.2 Earthquakes in Brazil

Brazil represents a relatively stable continental region, as mentioned. It is located far from the border with the African platform to the east; far from the Andean mountain range to the west; and the Caribbean mountain range to the north. In Brazil, earthquakes occur due to faults within the South American plate that contribute to the release of energy, producing seismic events. Despite being located in a stable region, the seismic study in Brazil has become important due to the presence of earthquakes far from the plate borders. These earthquakes are due to the dynamics of the faults within the South American plate. Most of the information that is available on the faults in Brazil comes from neotectonic studies, these vary depending on their location, such as in the Amazon region. Only a few faults have been studied recently. The platform where Brazil is located is made up of two types of

Figure 2.5: South American countries with high seismic hazard, described by Mercalli magnitude

Source: Regional Center of Seismology for South America(http://www.ceresis.org/ (07/06/2020)

Date	Magnitude(Mb)	Location
27/01/1922	5.1	Mogi Guaçu (São Paulo)
28/06/1939	5.1	Florianópolis (Santa Catarina)
1955	6.3	Vitória (Espírito Santo)
31/01/1955	6.6	Serra do Tombador (Mato Grosso)
28/02/1955	6.3	Vitoria (Espirito Santo)
20/11/1980	5.2	Pacajus (Fortaleza)
1983	5.5	Amazonas
30/11/1986	5.1	Joao Camara (Rio Grande do Norte)
23/03/2005	5.0	Portos dos Gaúchos (Mato Grosso)
21/07/2007	6.1	Cruzeiro do Sul (Acre)
23/04/2008	5.2	Plataform Continental
08/10/2010	5.0	Mara Rosa (Goiás)
15/05/2011	6.0	Rio Grande do Norte
24/08/2011	7.0	Acre, Amazonas
30/09/2012	7.1	Amazonas
05/06/2013	5.2	Acre
27/03/2014	5.1	Marechal Thaumaturgo (Acre)
07/04/2014	5.2	Tarauacá (Acre)
16/09/2015	6.5	Rio Grande do Sul
24/11/2015	7.6	Tarauacá (Acre)
26/11/2015	6.7	Tarauacá (Acre)
26/11/2015	5.1	Tarauacá (Acre)
18/04/2017	6.1	Manaus (Amazonas)
21/08/2018	7.3	Acre, Amapá, Amazonas, Pará, Roraima
05/01/2019	6.8	Tarauacá (Acre)
18/09/2020	6.9	Pernambuco
31/01/2021	5.7	Roraima, Amazonas

Table 2.2: Largest seismic events in Brazil (Centro de Sismologia da Universidade de São Paulo, Laboratório Sismológico da UFRN (LabSis/UFRN))

Precambrian Geotectonic units; cratonic blocks and collision sutures. The other important element is the shear guideline called, the Transbrazilian Lineament that extends 2,700 km across Brazilian territory, from the Ceará State in the northeast to the Mato Grosso do Sul State in the southwest. Table 2.1 shows the major seismic events in Brazil.

Figure 2.6 shows the active and potentially active Quaternary faults in Brazil. Many of these faults are considered evidence of the Quaternary movement, and they are related to long-lived linements or crustal discontinuities (SAADI et al., 2003).

All tremors that have occurred in Brazil are already cataloged on the page of the South and Southeast Brazil Seismographic Network - RSIS. It includes both ancient earthquakes studied only through historical, as well as recent accounts detected by seismographs. Of course, many other tremors have occurred in Brazil that were not cataloged, because they occurred in uninhabited regions or were not detected by seismographic stations due to the low intensity. The city of Monte Claros - MG, where the 2012 earthquake was recorded, is contained in a geological fault located in the northern

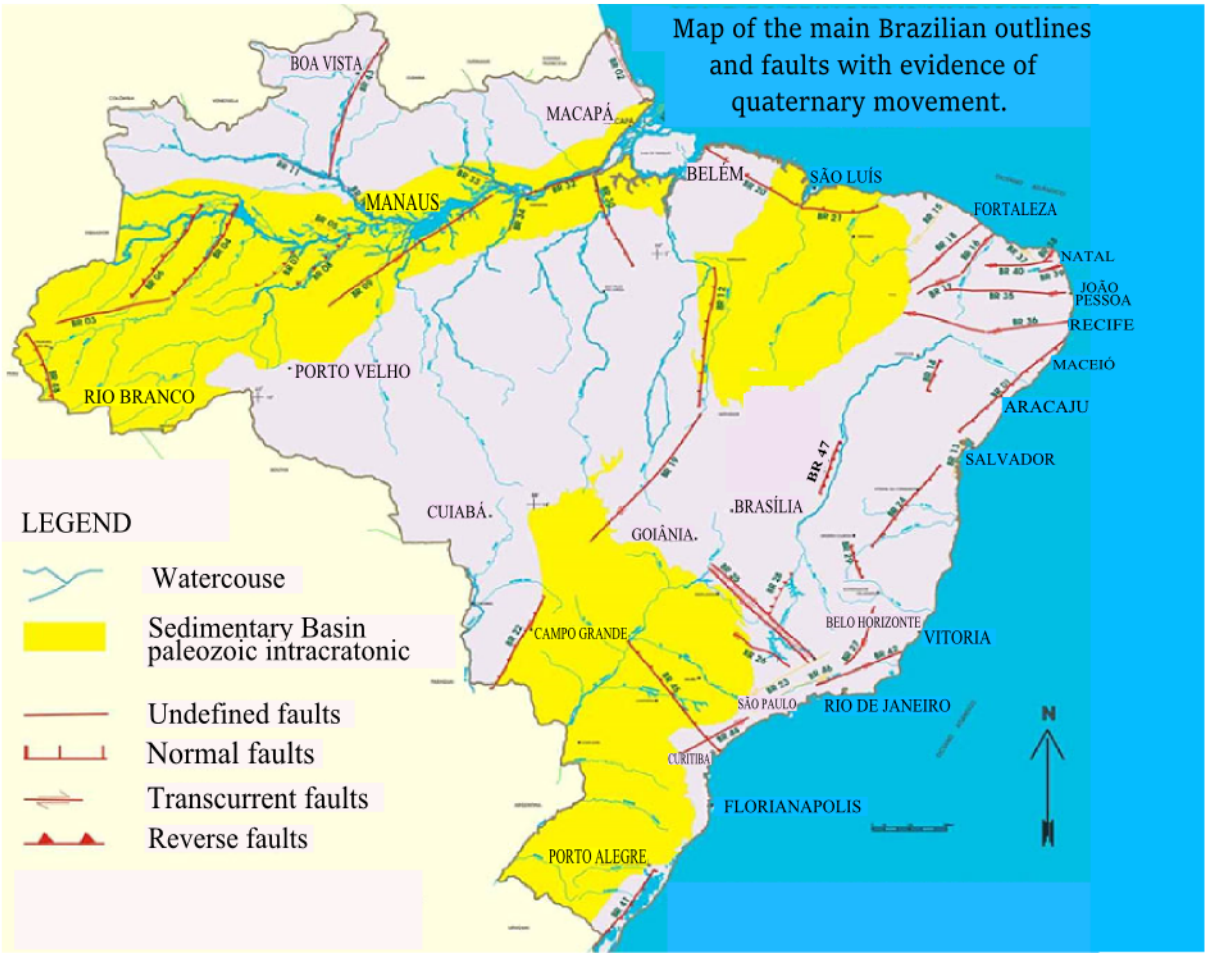

Figure 2.6: Main geological faults in the Brazilian territory
Source: Adapted from (SAADI et al., 2003)

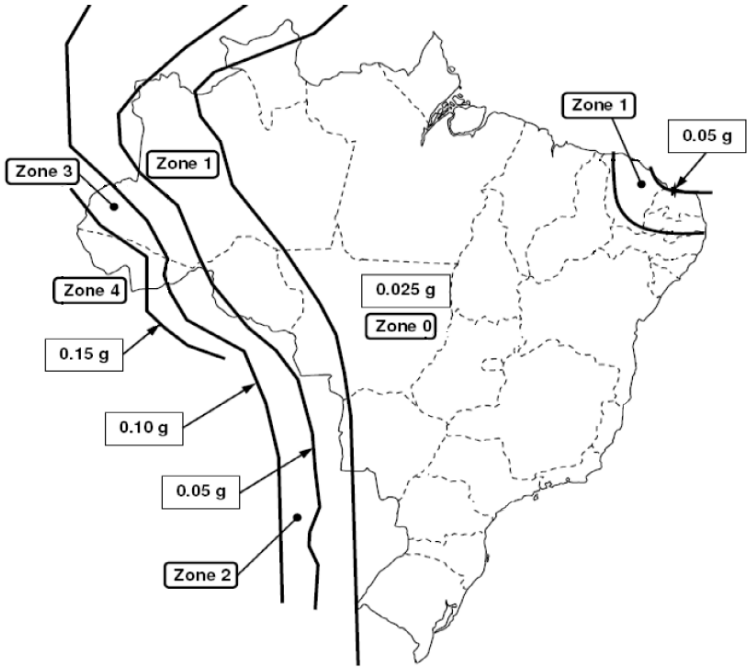

Figure 2.7: Brazil risk seismic zones, with Zone 4 being the highest risk and Zone 0 having the least risk.

Source: Adapted from (SANTOS et al., 2008)

state of Minas Gerais, corresponding to line number 47 indicated on the map illustrated in Figure 2.3. Regarding recent earthquakes, Montes Claros stands out as one of the cities with the highest recurrence of earthquakes in Brazil (ASSUMPÇÃO; NETO, 2000)

In Brazil the seismic hazard is low for the southwestern areas of the population, but for areas in the northwest the seismic hazard is not negligible, because it is in contact with the fault of the Central Atlantic. This led to the need to create a seismic zoning map with the help of some data obtained from neighboring countries. This map shows the accelerations that occur on the South American continent.

In Figure 2.7, the zones representing the accelerations Ag are presented. It is observed that for Zone 4: $Ag \geq 0,15g$, and Zone 3: $0.1g \leq Ag \leq 0.15g$ which represent a seismic potential for Acre and west of Amazonas states. Zone 2: $0.05g \leq Ag \leq 0.1g$ and Zone 0: $Ag \leq 0.025g$ to west and northeast of Brazil (SANTOS et al., 2010).

2.6 SEISMIC WAVES

As seen previously, fractures in the tectonic plates when moving, produce energy waves, which can be captured by the seismographic stations located near the faults. This information is used for research on the composition of the Earth's interior. The types of waves that are recorded are the body waves and the surface waves which are represented by seismograms. The seismograms describe the primary and secondary waves at the arrival time, being able to verify the existence of these types of

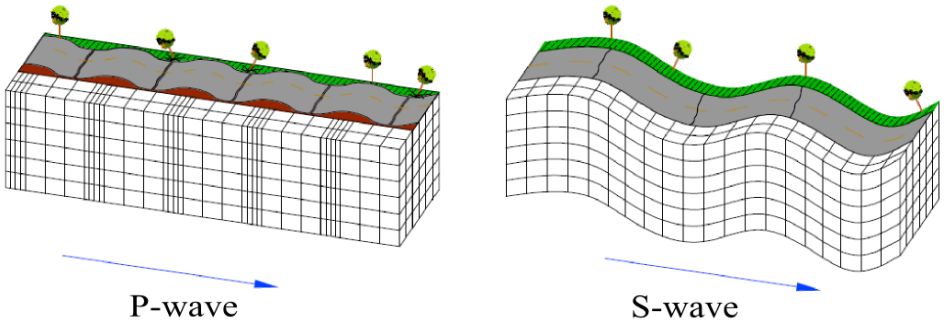

Figure 2.8: Body Waves. First figure: P-waves, where the movement of particles is parallel to the direction of wave propagation. Second figure: S-waves, where the movement of the particles are perpendicular to the direction of wave propagation
Source: Adapted from (GARCIA et al., 2018)

waves that will be defined below.

2.6.1 Body Waves

The Earth being an elastic solid, two types of waves are produced; compressional waves, or P waves, and transversal waves, or S waves, Figure 2.8. The P wave is the fastest, the movement of particles is parallel to the direction of wave propagation, as successive compressions and dilations. It can also originate from a combination of seismic waves caused by reflections and refractions. On the contrary, the S waves arrive at the seismographs after the P waves. The movement of the particles are perpendicular to the direction of the wave, so it is polarized in horizontal motion SH and vertical movement SV.

When the primary or body waves reach the surface, it travels along the Earth as surface waves, which generally cause catastrophic effects.

2.6.2 Surface Waves

There are two types of waves that propagates around litters of different materials, in regions of a high gradient of speed and density close to the surface, Figure 2.9. The Rayleigh wave LR, where the trajectories of the particles are ellipses, their largest axes are vertical and the smaller ones are in the direction of wave propagation. The Love waves LQ are of the SH type, the movement of the particles is horizontal and normal to the direction of propagation, it needs a waveguide that is the surface of the Earth.

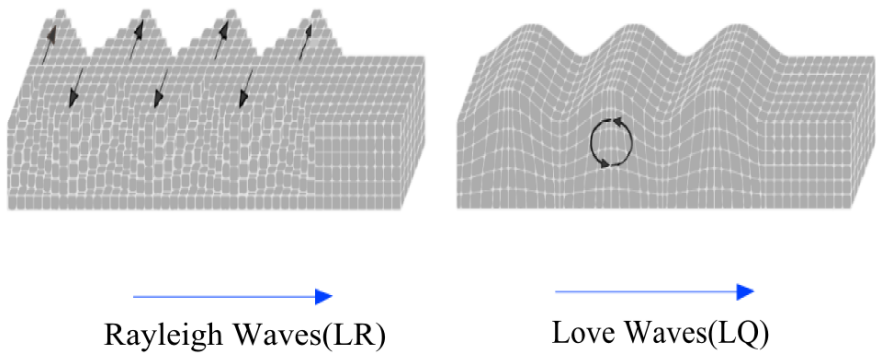

Figure 2.9: Surface waves. First figure: In LR-waves the trajectories of the particles are ellipses. Second figure: In LQ-waves the movement of the particles is horizontal and normal to the direction of propagation

Source: Adapted from (GATES, et al., 2006)

3 EARTHQUAKE MODELLING

In this chapter the modeling of seismic waves is developed. In the first part, the works carried out over the recent decades are presented for the modeling of P, SV and SH waves with different perspectives in terms of earthquake sources, domain, discretization, interfaces and specific difficulties that were solved. Regarding the elements that characterize the phenomenon, at the end of the first section the elements that will be used in this work for the modeling of P-SV seismic waves are mentioned. In the second part, the modeling of the problem is presented using physical and mathematical tools such as Newton's laws and the relationships between stress and strain given by Hooke's generalized law, particularizing for an isotropic medium, obtaining the system of P-SV equations for a continuous medium. Due to the characteristics of the problem, that is, describing shallow earthquakes, in the third part of the chapter we model the domain as a rectangular region. In the last part, the initial and border conditions are given. Due to the partition of the domain, the boundary conditions are free to avoid reflections. For initial conditions, displacements and speeds are null, while a source is used as an instantaneous initial force.

3.1 REVIEW OF P AND SV SEISMIC WAVE MODELING

Mathematical models to explain the propagation of seismic waves carry common elements. The medium in which the seismic waves propagate can be an isotropic or anisotropic medium, the latter being more complicated to simulate due to the modeling of elastic constants. Another element is that the equations have not exact solution. The domain in which these equations are defined is finite and discretized, leading to the use of suitable boundary conditions. It is important to reduce the reflections that are produced by the boundaries of the domain. The border that is in contact with the air, called the free surface, is where the movements that modify the geography take place. Strata and geological discontinuities can be considered interfaces, since there is a change in physical properties of the layers. The hypocenter of the earthquake also is known as source. Different speeds are presented for each medium, which is greater with depth. Also in each of these interfaces there are reflections and diffractions. The seismic waves can be of the P, SV or SH type which can also be produced at the interfaces by diffractions and reflections.

One of the first mathematical models to explain the propagation of elastic waves carried out by Pekeris et al. (1965), they used the exact Ray theory to solve the propagation of a compression source, for elastic media with an interface, where the reflections are produced. The work was described to diferent Lame's constants and velocities in each medium. The numerical calculation time was too long so, Alterman and Karal (1968) introduce the Finite Difference Method (FDM) to solve the elastic wave equations. They used a medium with an interface and a point source, using boundary conditions on the free surface and at the interface. They studied also the refraction of the Rayleigh wave at the surface and at the interface. They obtained numerical solutions, which showed the vertical and horizontal displace-

ment, represented by theoretical seismograms. For a propagation of a elastic wave in a semi-infinite medium, Alterman and Karal (1970) used a pulse to model the effects of a source using FDM. They showed graphs to demonstrate the displacement, stresses and strains for different levels in the pulse. The seismic wave approach carried out by Virieux (1986), performed the modeling for P-SV seismic waves for a heterogeneous medium using the velocity-stress, where the interface was represented by changes on density and elastic parameters. It was used a Gaussian function as a source. The wave propagation in porous solid media was worked by Vashisth and Gogna (1993). They assumed the stresses continuous, a linear relationship between the shear-stresses, and the slip through the interface. Numerical solutions was obtained that showed the energy attenuation for different parameters.

In the following decade, another type of approach was used for seismic waves, as well as the improvement in the precision of the models presented in the previous works. Hustedt et al. (2004) solved the acoustic wave equation. They used mixed grid and Staggered grid Finite Difference Method (SFDM) for frequency domain acoustic wave. The precision of the fourth-order staggered mesh is slightly higher than the mixed mesh. In the case of seismic wave in irregular free surface, Zhang et al. (2006) proposed Traction Image Method (TIM) for irregular free surface boundaries in finite differences. The grid is defined by a curvilinear coordinate system, in which the velocity-stress equations are updated numerically using an optimized high-order non-staggered finite difference scheme. To satisfy the boundary conditions of the free surface, the Traction Image Method is extended for a flat surface, it is also used for an arbitrary irregular surface. The acoustic wave was also used by Fernandes et al. (2009) to model seismic waves in the Bacia Amazonica. The FDM Where the FDM was used to obtain the P and S wavefield. They use irregular interfaces getting reflections, and diffractions in each media given by different physical properties. The amount of time for solving the seismic wave equation given by the FDM is quite long for smaller amplitudes.

In the following years, techniques were developed to decrease the calculation time in order to extend the domain for the seismic waves. Silva et al. (2009) proposed to parallelize the solutions using finite differences time-domain algorithm. They used an interleaved mesh to guarantee stability and have better efficiency in the temporal domain. To model seismic waves on a large scale, Virieux et al. (2012) used two techniques for solving the elastodynamic equations, Finite Difference Method (FDM) and Finite Element Method (FEM), both in the time and frequency domain. They used free boundary and attenuation conditions. For the three-dimensional seismic wave behavior, Contreras et al. (2012) used the elastodynamic equations in a solid-fluid media, where the interface is modeled by an implicit condition. The FDM was used to solve the velocity stress and displacement stress equations.

In the next years, the technique has been improved numerically with the introduction of numerical meshes that adapt to complex borders and domains, optimizing the calculation time for the solution. For P and S wave simulations using both the first and second order separated wave equations.

Bai et al. (2013) made an instantaneous comparison of the two types of approaches for the seismic phenomenon. In both cases, the SFDM was used with different order of precision. To reduce the number of calculations in uniform grid, Zhang et al. (2013) implement a discontinuous grid for the simulation of seismic waves. The FDM is used on curvilinear coordinates. They obtained a method that can simulate large-scale, high-frequency earthquakes considering the region topography. Alcrudo (2014) used the Sofi2D, a program based on elastic and viscoelastic wave modeling resolved numerically by the FDM to model seismic waves with transparent boundary conditions, with and an interface given by the physical properties of the medium. For a complex free surface topography, Lisitsa et al. (2016) developed a hybrid algorithm to simulate seismic waves from combination of the FDM and the Garlekin discontinuous method. Takenaka et al. (2017) solved the three-dimensional sub-global model using the elastic waves without anelastic attenuation in a spherical polar coordinate. To model the propagation of 2-D seismic waves for an irregular domain, Benito et al. (2017) used the Generalized Finite Difference Method (GFDM) for solve the velocity stress and displacement equations. The absorbing boundaries have been modeled with Perfectly Matched Layers (PML). Ren et al. (2019) proposed an implicit Staggered-grid Finite Difference scheme with a combined stencil. The combination of cross and rhombus stencils for 2-D wave equation and a combination of cross and pyramid stencils for 3-D.

In this context, this work describes the propagation of P and SV seismic waves with attenuation term modeled by the equations of motion in elastic media. The partial differential equations (PDE) describe the propagation in homogeneous media. Neuman's condition is used for the free surface. For the source, a Dirac Delta function is used. To solve this PDE system, the FDM is used to approximate second-order derivatives in space and time, and cross derivatives to space. Boundary conditions are also discretized by FDM.

3.2 P AND SV SEISMIC WAVE MODELING WITH ATTENUATION

The mathematical modeling will be performed in a homogeneous medium. It means that our medium is isotropic for the Lame constants. Terrestrial layers can be described by means of their elastic properties. The propagation of mechanical waves is polarized, being the P and SV waves independent of SH. The modeling of this type of wave will be described below.

As seismic waves are time dependent, so we need to know the effects at the linear momentum, because it implies variations in velocities and accelerations. We apply Newton's law to a continuous medium, considering normal and shear stress in an infinitesimal cube Figure 3.1 with coordinates (x, y, z).

The total set of forces on each side of a cube is represented as;

$$F_i = \sum_{j=1}^{3} \frac{\partial \tau_{ij}}{\partial x_j} dx_1\, dx_2\, dx_3 \tag{3.1}$$

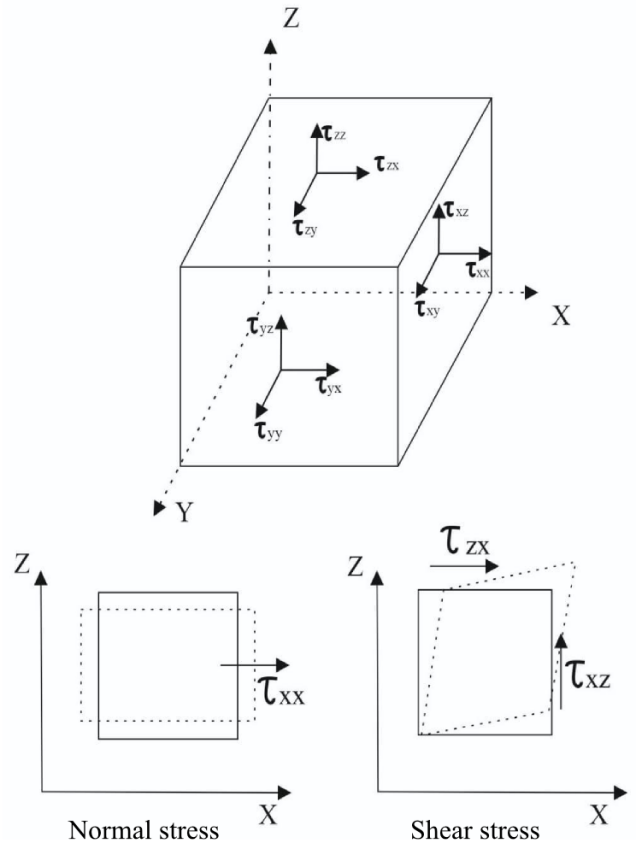

Figure 3.1: Decomposition of forces on each face of the cube
Source: Adapted from (BECERRA, 2011)

or, using sum notation over repeated indices,

$$F_i = \partial_j \tau_{ij}\ dx_1\, dx_2\, dx_3. \tag{3.2}$$

There are also external forces acting on the cube, which are proportional to the volume of the material

$$(F)_i^{body} = f_i dx_1 dx_2 dx_3. \tag{3.3}$$

The mass in an infitesimal cube is given by the following equation;

$$m = \rho\, dx_1 dx_2 dx_3, \tag{3.4}$$

where ρ is the density. Due to Newton's second law, the momentum change is proportional to the forces acting on the region, Figure 3.1. So, getting the acceleration by deriving the displacement twice, and then substituting in Newton's formula, $F = ma$, obtain

$$\rho\, \frac{\partial^2 u_i}{\partial t^2} = \partial_j \tau_{ij} + f_i. \tag{3.5}$$

This is the fundamental equation in seismology known as the equation of motion for a continuous medium, where u_i, τ_{ij} are displacement, strain and f usually is a gravity (f_g) and source.

In our work, we consider an external dissipative force acting on stress and strain processes called attenuation

$$f_i = -\gamma_i \frac{\partial u_i}{\partial t}. \tag{3.6}$$

The relationship between stress and strain is given in terms of the displacement u, given by Hooke's general law. In an isotropic body, where the properties do not depend on direction, the relationship reduces to

$$\tau_{ij} = \lambda \delta_{ij} \partial_k u_k + \mu(\partial_i u_j + \partial_j u_i), \tag{3.7}$$

where λ and μ are the Lame parameters and δ_{ij} is the Kronecker delta. Equations (3.5), (3.6) and (3.7) are used to model the propagation of seismic waves, stress and displacement. For the 2-D case, only the x and z plane will be considered, because this is where the propagation of the P-SV waves are considered, so in the equation (3.5) and (3.7) the derivative terms $\dfrac{\partial}{\partial y}$ are null. Figure 3.2 shows the direction in which the P and SV waves are propagated.

Now considering the forces in $\mathbf{u} = (\mathbf{u_x}, \mathbf{0}, \mathbf{u_z})$ only on the x, z axes. Using the equation (3.5), and (3.6)

$$\rho \frac{\partial^2 u_x}{\partial t^2} = \partial_j \tau_{xj} = \frac{\partial \tau_{xx}}{\partial x} + \frac{\partial \tau_{xz}}{\partial z} - \gamma_1 \frac{\partial u_x}{\partial t} \tag{3.8}$$

$$\rho \frac{\partial^2 u_z}{\partial t^2} = \partial_j \tau_{zj} = \frac{\partial \tau_{xz}}{\partial x} + \frac{\partial \tau_{zz}}{\partial z} - \gamma_2 \frac{\partial u_z}{\partial t}. \tag{3.9}$$

By the equation (3.7) the stress τ_{xx}, τ_{xz} and τ_{zz} are given by

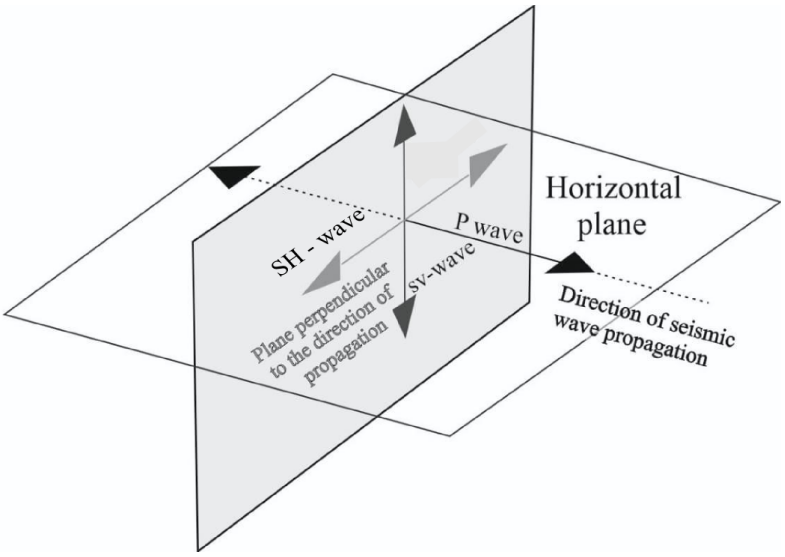

Figure 3.2: Seismic waves direction. SH: Displacements in the horizontal plane and SV: Displacements in the perpendicular plane to SH
Source:Adapted from (ROSA FILHO et al., 2003)

$$\tau_{xx} = \lambda\left[\frac{\partial u_x}{\partial x} + \frac{\partial u_z}{\partial z}\right] + \mu\left[2\frac{\partial u_x}{\partial x}\right]$$

$$\tau_{xx} = (\lambda + 2\mu)\frac{\partial u_x}{\partial x} + \lambda\frac{\partial u_z}{\partial z} \tag{3.10}$$

$$\tau_{xz} = \mu\left[\frac{\partial u_x}{\partial z} + \frac{\partial u_z}{\partial x}\right] \tag{3.11}$$

$$\tau_{zz} = \lambda\left[\frac{\partial u_x}{\partial x} + \frac{\partial u_z}{\partial z}\right] + \mu\left[2\frac{\partial u_z}{\partial z}\right]$$

$$\tau_{zz} = (\lambda + 2\mu)\frac{\partial u_z}{\partial z} + \lambda\frac{\partial u_x}{\partial x}. \tag{3.12}$$

They are the equations that model the P-SV waves, where the terms λ and μ e are Lame's parameters considered constants.

Replacing terms (3.10) and (3.11) in (3.8)

$$\rho\frac{\partial^2 u_x}{\partial t^2} = \frac{\partial}{\partial x}\left(\lambda\left[\frac{\partial u_x}{\partial x} + \frac{\partial u_z}{\partial z}\right] + \mu\left[2\frac{\partial u_x}{\partial x}\right]\right) + \frac{\partial}{\partial z}\left(\mu\left[\frac{\partial u_x}{\partial z} + \frac{\partial u_z}{\partial x}\right]\right) - \gamma_1\frac{\partial u_x}{\partial t},$$

and regrouping the terms

$$\rho\frac{\partial^2 u_x}{\partial t^2} = (\lambda+2\mu)\frac{\partial^2 u_x}{\partial x^2} + \mu\frac{\partial^2 u_x}{\partial z^2} + (\lambda+\mu)\frac{\partial^2 u_z}{\partial z \partial x} - \gamma_1\frac{\partial u_x}{\partial t}. \tag{3.13}$$

.

Similarly, replacing (3.11) and (3.12) in (3.9)

$$\rho\frac{\partial^2 u_z}{\partial t^2} = \frac{\partial}{\partial z}\left(\lambda\left[\frac{\partial u_x}{\partial x} + \frac{\partial u_z}{\partial z}\right] + \mu\left[2\frac{\partial u_z}{\partial z}\right]\right) + \frac{\partial}{\partial x}\left(\mu\left[\frac{\partial u_x}{\partial z} + \frac{\partial u_z}{\partial x}\right]\right) - \gamma_2\frac{\partial u_z}{\partial t},$$

we obtain

$$\rho\frac{\partial^2 u_z}{\partial t^2} \quad = \quad (\lambda+2\mu)\frac{\partial^2 u_z}{\partial z^2} + \mu\frac{\partial^2 u_z}{\partial x^2} + (\lambda+\mu)\frac{\partial^2 u_x}{\partial z \partial x} - \gamma_2\frac{\partial u_z}{\partial t}, \tag{3.14}$$

(RICHARDS, AKI, 1980; VIRIEUX, 1986).

The system of equations (3.13) and (3.14) describe the P-SV seismic waves with dispersion and attenuation. In the next section we see the characteristics of the domain on its borders.

3.3 GEOMETRIC DOMAIN

The domain is a very relevant topic in the study since the model will describe earthquakes near the surface, and when comparing this depth of the earthquake with the size of the earth's radius it is possible to choose a rectangular domain. Earthquakes in Brazil occur at a depth less than or equal to 50km, while the radius of the earth is 6371km. The Figure 3.3 show the domain that is very close to the free surface, where the source will be placed. In this configuration, we will use Cartesian coordinates to model the propagation of that source.

The seismic wave equations are modeled for an unlimited and infinite domain Ω_∞ and also that it has no analytical solutions, so the use of numerical methods is essential for its solution, such as the finite difference method. On the other hand, the domain of our problem is limited. The Figure 3.4 represents a close-up of the domain designed in Figure 3.3. Note that at the edges of our computational domain, Figures 3.4 and 3.5, we must impose Neumann-type conditions, so that the waves pass through the boundary of the computational domain.

3.4 INITIAL AND BOUNDARY CONDITIONS

Non-reflective boundary conditions will be used, because the waves naturally in that domain would be continuous and without limits. Segments B1, B2, B3, and B4 are the computational limit of the domain. In the Figure 3.5, it shows the four bondaries, which can be understood as a vertical domain located within the Earth.

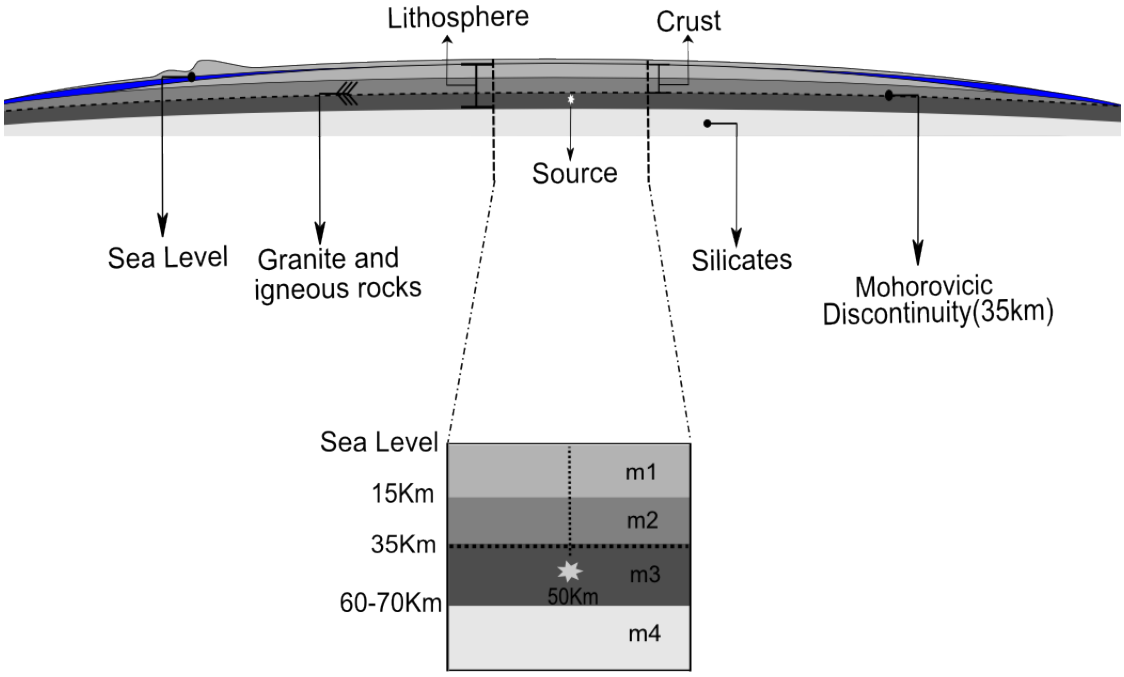

Figure 3.3: Domain location near the Earth's surface
Source: Author

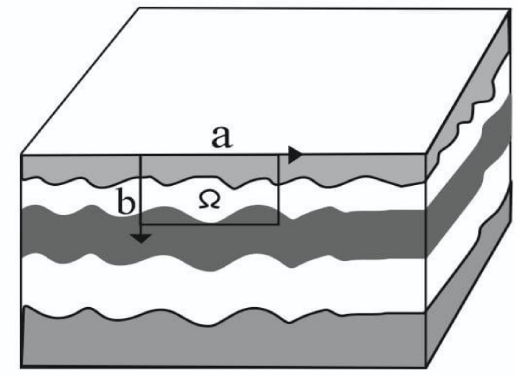

Figure 3.4: Schematic representation of the vertical computational domain Ω with lengths **a** and **b**, inside the Earth
Source: Adapted from (BECERRA, 2011)

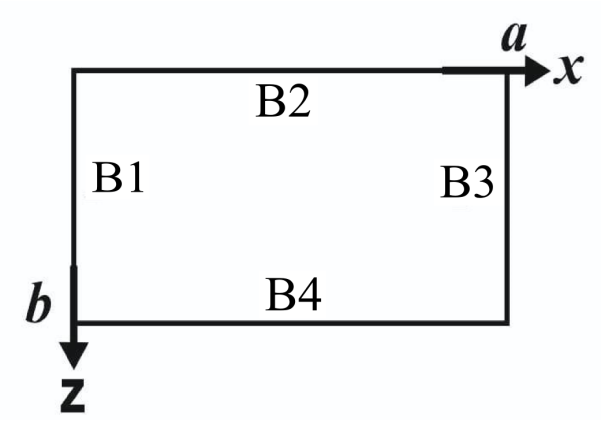

Figure 3.5: Labeling the borders in the vertical computational domain Ω with lengths a and b
Source: Author

The use of fixed boundary conditions (Dirichelet conditions) result in a reflection of the inverted phase of the wave, as opposed to a free boundary conditions (Neumann conditions). To the border on the Earth's surface ($B2$ border), Robin's condition is used.

For the equation u_x, the Neumann conditions are used

$$\frac{\partial u_x(B3)}{\partial n} = \frac{\partial u_x(B4)}{\partial n} = \frac{\partial u_x(B1)}{\partial n} = \frac{\partial u_x(B2)}{\partial n} = 0. \tag{3.15}$$

For the equation u_z, is also used the Neumann conditions to avoid reflections

$$\begin{aligned} \frac{\partial u_z(B3)}{\partial n} = \frac{\partial u_z(B4)}{\partial n} = & \frac{\partial u_z(B1)}{\partial n} = 0 \\ \frac{\partial u_z(B2)}{\partial n} = & \dot{Q}. \end{aligned} \tag{3.16}$$

For the initial condition, the medium is considered to be in a steady state, then we enforce that within the domain have to

$$u_x(x, z, t) = 0, \qquad t = 0 \tag{3.17}$$

$$u_z(x, z, t) = 0, \qquad t = 0. \tag{3.18}$$

The source can be introduced as an initial condition or a force in the differential equations, which disturbs the medium at first. In the literature there are functions that model this phenomenon, one of which is the Gaussian function. In our mathematical modeling of the problem, we consider a Gaussin-type source added as an external force in the differential equations of motion. The source is centered at the position (x_0, z_0), but distributed over an area given by the Gaussian function. We add the following bodyforce for the two-dimensional P-SV system

$$\begin{aligned} E_x(x,z,t) &= a_1 e^{-c_1 t^2} \times e^{-\kappa_1[(x-x_0)^2+(z-z_0)^2]} \\ E_z(x,z,t) &= a_2 e^{-c_2 t^2} \times e^{-\kappa_2[(x-x_0)^2+(z-z_0)^2]}. \end{aligned} \tag{3.19}$$

In the first simulations, due to the homogeneity of the medium, we will consider that

$$a_1 = a_2 = a$$
$$\kappa_1 = \kappa_2 = \kappa.$$

In the next section we will obtain the discretized equations that model the seismic waves for a computational domain, as well as their initial and boundary conditions.

4 NUMERICAL MODEL

In this chapter the equations will be discussed in their discrete form, this means that discretization methods will be used to transform the equations given in the previous chapter. In the first part, the domain is discretized by means of a Cartesian mesh, where each point is an approximation of the solution for that point. In the second part, the central and backward finite difference scheme is used for the spatial and temporal derivatives respectively, generating an implicit scheme, leading to the resolution of a linear system. As well as the model equations, the initial and boundary conditions are also discretized, at each point and by central finite differences, generating the conditions for domain interior points at the initial time and the edge of the points for all times. In the last part the consistency analysis of the discretized equation is developed, this to be sure that the discretized system of equations corresponds to the continuous equations to be solved, that is, the P-SV system (3.13 - 3.14).

4.1 DOMAIN DISCRETIZATION

For the domain where the finite difference method will be applied, a rectangular spatial discretization is used, as shown in Figure 4.1. It is called the computational mesh, where the displacements u_x and u_z are calculated numerically only at their points $u_x(x_i, z_k)$ and $u_z(x_i, z_k)$.

4.2 MODEL DISCRETIZATION

For the solution of P-SV system (3.13-3.14), a numerical scheme given in finite differences, as given by Figure 4.2, which will give us an approximation to the solution of the problem in time $(l+1)$ and in position (i, k).

$$\rho\frac{\partial^2 u_x}{\partial t^2}\Big|_{i,k}^{l+1} = (\lambda+2\mu)\frac{\partial^2 u_x}{\partial x^2}\Big|_{i,k}^{l+1} + \mu\frac{\partial^2 u_x}{\partial z^2}\Big|_{i,k}^{l+1} + (\lambda+\mu)\frac{\partial^2 u_z}{\partial z\partial x}\Big|_{i,k}^{l+1} - \gamma_1\frac{\partial u_x}{\partial t}\Big|_{i,k}^{l+1} + E_x\Big|_{i,k}^{l+1} \tag{4.1}$$

$$\rho\frac{\partial^2 u_z}{\partial t^2}\Big|_{i,k}^{l+1} = (\lambda+2\mu)\frac{\partial^2 u_z}{\partial z^2}\Big|_{i,k}^{l+1} + \mu\frac{\partial^2 u_z}{\partial x^2}\Big|_{i,k}^{l+1} + (\lambda+\mu)\frac{\partial^2 u_x}{\partial z\partial x}\Big|_{i,k}^{l+1} - \gamma_2\frac{\partial u_z}{\partial t}\Big|_{i,k}^{l+1} + E_z\Big|_{i,k}^{l+1} \tag{4.2}$$

4.2.1 Discretization of the equation Ux

First, the x-displacement equation (4.1) will be discretized using the finite differences method. For spatial derivatives, the central difference scheme is used, while for time derivatives, the backward difference scheme is used. Note that all approximations are second order. Applying this methodology to the derivatives in (4.1), the reference point is $u_x\Big|_{i,k}^{l+1}$

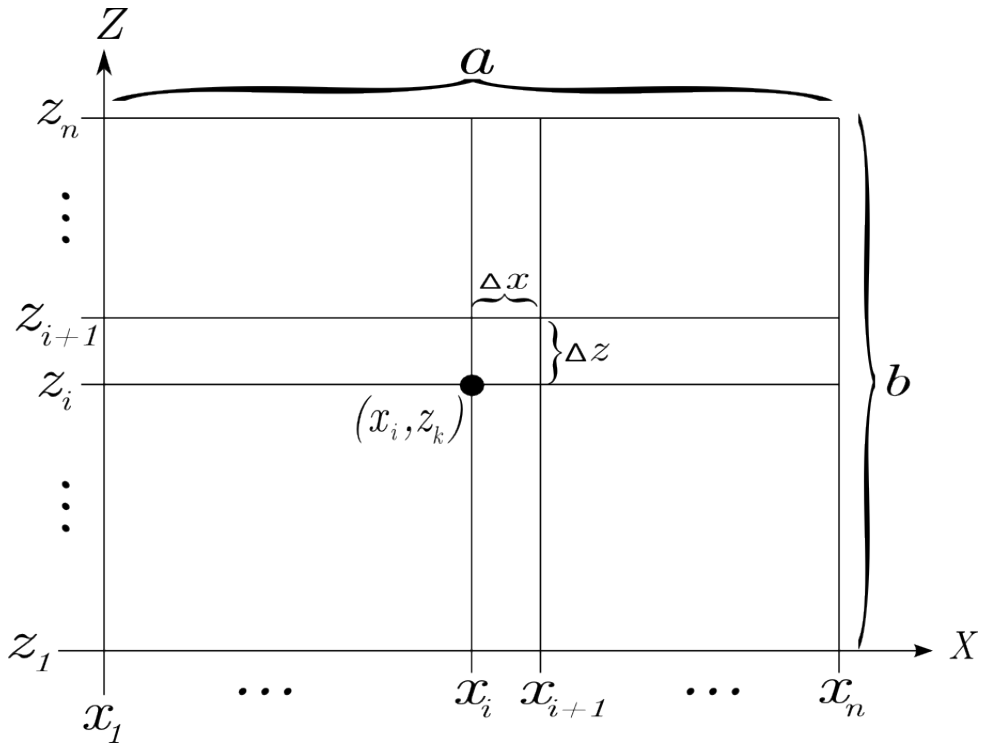

Figure 4.1: Mesh points for numerical solution
Source: Author

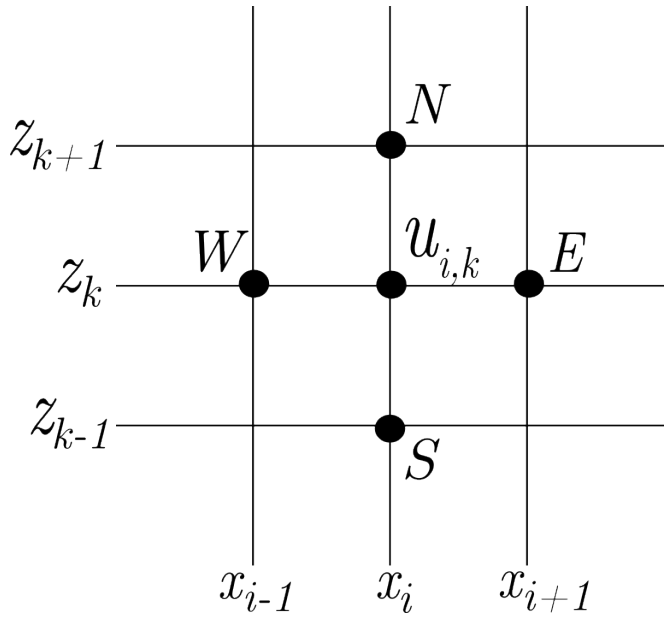

Figure 4.2: Computational nodes and cardinal points
Source: Author

$$\begin{aligned}\frac{\rho}{\triangle t^2}\left[u_x{}_{i,k}^{l+1}-2u_x{}_{i,k}^{l}+u_x{}_{i,k}^{l-1}\right] &= \frac{\lambda+2\mu}{\triangle x^2}\left[u_x{}_{i+1,k}^{l+1}-2u_x{}_{i,k}^{l+1}+u_x{}_{i-1,k}^{l+1}\right]\\ &+\frac{\mu}{\triangle z^2}\left[u_x{}_{i,k+1}^{l+1}-2u_x{}_{i,k}^{l+1}+u_x{}_{i,k-1}^{l+1}\right]\\ &+\frac{\lambda+\mu}{4\triangle x\triangle z}\left[u_z{}_{i+1,k+1}^{l+1}-u_z{}_{i+1,k-1}^{l+1}+u_z{}_{i-1,k-1}^{l+1}-u_z{}_{i-1,k+1}^{l+1}\right]\\ &-\frac{\gamma_1}{2\triangle t}\left[3u_x{}_{i,k}^{l+1}-4u_x{}_{i,k}^{l}+u_x{}_{i,k}^{l-1}\right]+a_1e^{-c_1(t_{l+1})^2}e^{-\kappa_1(x_i^2+z_k^2)}.\end{aligned} \tag{4.3}$$

$$\begin{aligned}\left(\frac{\rho}{\triangle t^2}+\frac{3\gamma_1}{2\triangle t}+\frac{2(\lambda+2\mu)}{\triangle x^2}+\frac{2\mu}{\triangle z^2}\right)u_x{}_{i,k}^{l+1} &= \left(\frac{2\rho}{\triangle t^2}+\frac{4\gamma_1}{2\triangle t}\right)u_x{}_{i,k}^{l}-\left(\frac{\rho}{\triangle t^2}+\frac{\gamma_1}{2\triangle t}\right)u_x{}_{i,k}^{l-1}\\ &+\frac{\lambda+2\mu}{\triangle x^2}\left[u_x{}_{i+1,k}^{l+1}+u_x{}_{i-1,k}^{l+1}\right]+\frac{\mu}{\triangle z^2}\left[u_x{}_{i,k+1}^{l+1}+u_x{}_{i,k-1}^{l+1}\right]\\ &+\frac{\lambda+\mu}{4\triangle x\triangle z}\left[u_z{}_{i+1,k+1}^{l+1}-u_z{}_{i+1,k-1}^{l+1}+u_z{}_{i-1,k-1}^{l+1}-u_z{}_{i-1,k+1}^{l+1}\right]\\ &+a_1e^{-c_1(t_{l+1})^2}e^{-\kappa_1(x_i^2+z_k^2)}.\end{aligned} \tag{4.4}$$

We denoted some of the terms like:

$$\begin{aligned}A_{P1} &= \frac{\rho}{\triangle t^2}+\frac{3\gamma_1}{2\triangle t}+\frac{2(\lambda+2\mu)}{\triangle x^2}+\frac{2\mu}{\triangle z^2}\\ A_{E1} &= A_{W1}=\frac{\lambda+2\mu}{\triangle x^2}\\ A_{N1} &= A_{S1}=\frac{\mu}{\triangle z^2}\\ b1 &= \left(\frac{2\rho}{\triangle t^2}+\frac{4\gamma_1}{2\triangle t}\right)u_x{}_{i,k}^{l}-\left(\frac{\rho}{\triangle t^2}+\frac{\gamma_1}{2\triangle t}\right)u_x{}_{i,k}^{l-1}\\ ACu_z^{l+1} &= \frac{\lambda+\mu}{4\triangle x\triangle z}\left[u_z{}_{i+1,k+1}^{l+1}-u_z{}_{i+1,k-1}^{l+1}+u_z{}_{i-1,k-1}^{l+1}-u_z{}_{i-1,k+1}^{l+1}\right],\end{aligned} \tag{4.5}$$

then, replacing (4.5) in (4.4), we have

$$\begin{aligned}u_x{}_{i,k}^{l+1} = \frac{1}{A_{P1}}\Big[&A_{E1}u_x{}_{i+1,k}^{l+1}+A_{W1}u_x{}_{i-1,k}^{l+1}+A_{N1}u_x{}_{i,k+1}^{l+1}+A_{S1}u_x{}_{i,k-1}^{l+1}+b1+ACu_z^{l+1}+\\ &+a_1e^{-c_1(t_{l+1})^2}e^{-\kappa_1(x_i^2+z_k^2)}\Big].\end{aligned} \tag{4.6}$$

Observe that the Equation (4.6) results in an implicit scheme, therefore it results in a system of equations, which is expressed in blocks of tridiagonal matrices. Thus obtaining the system of linear equations given by

$$A_1u_x = B_1 \tag{4.7}$$

which denotes the system to be solved.

$$\underbrace{\begin{bmatrix} A_{P1}-A_{N1} & -A_{E1} & & & & & & \\ -A_{S1}A_{P1}-A_{N1} & -A_{E1} & & & & & & \\ \ddots & \ddots & \ddots & \ddots & & & & \\ -A_{S1}A_{P1}-A_{N1} & -A_{E1} & & & & & & \\ -A_{S1}A_{P1} & -A_{E1} & & & & & & \\ \ddots & \ddots & \ddots & \ddots & & & & \\ & & & -A_{W1}A_{P1}-A_{N1} & & & & \\ & & & -A_{W1}-A_{S1}A_{P1}-A_{N1} & & & & \\ & & & \ddots & \ddots & \ddots & \ddots & \\ & & & -A_{W1}-A_{S1}A_{P1}-A_{N1} & & & & \\ & & & -A_{W1} & -A_{S1}A_{P1} & & & \end{bmatrix}}_{A_1} \cdot \underbrace{\begin{bmatrix} u_x{}_{2,2}^{l+1} \\ u_x{}_{2,3}^{l+1} \\ \vdots \\ u_x{}_{2,n-2}^{l+1} \\ u_x{}_{2,n-1}^{l+1} \\ \vdots \\ u_x{}_{n-1,2}^{l+1} \\ u_x{}_{n-1,3}^{l+1} \\ \vdots \\ u_x{}_{n-1,n-2}^{l+1} \\ u_x{}_{n-1,n-1}^{l+1} \end{bmatrix}}_{u_x} =$$

$$= \underbrace{\begin{bmatrix} b1_{2,2}+ACu_z{}_{2,2}^{l+1}+A_{W1}u_x{}_{2,1}^{l+1}+A_{S1}u_x{}_{1,2}^{l+1} \\ b1_{2,3}+ACu_z{}_{2,3}^{l+1}+A_{W1}u_x{}_{1,3}^{l+1} \\ \vdots \\ b1_{2,n-2}+ACu_z{}_{2,n-2}^{l+1}+A_{W1}u_x{}_{1,n-2}^{l+1} \\ b1_{2,n-1}+ACu_z{}_{2,n-1}^{l+1}+A_{W1}u_x{}_{2,n}^{l+1}+A_{N1}u_x{}_{1,n-1}^{l+1} \\ \vdots \\ b1_{n-1,2}+ACu_z{}_{n-1,2}^{l+1}+A_{E1}u_x{}_{n-1,1}^{l+1}+A_{S1}u_x{}_{n,2}^{l+1} \\ b1_{n-1,3}+ACu_z{}_{n-1,3}^{l+1}+A_{E1}u_x{}_{n,3}^{l+1} \\ \vdots \\ b1_{n-1,n-2}+ACu_z{}_{n-1,n-2}^{l+1}+A_{E1}u_x{}_{n,n-2}^{l+1} \\ b1_{n-1,n-1}+ACu_z{}_{n-1,n-1}^{l+1}+A_{E1}u_x{}_{n,n-1}^{l+1}+A_{N1}u_x{}_{n-1,n}^{l+1} \end{bmatrix}}_{B_1}, \tag{4.8}$$

this matrix (4.8) give us the points $u_{xi,k}$ within the grid, and the other points are boundary conditions make up the coefficient matrix B_1.

4.2.2 Discretization of the equation Uz

Now, the z-displacement equation (4.2) will be discretized using the finite differences method. Again, for spatial derivatives, the central difference scheme is used, while for time derivatives, the backward difference scheme is used. Note that all approximations are second order. Applying this methodology to the derivatives in (4.2) and the reference point is $u_z\Big|_{i,k}^{l+1}$

$$\begin{aligned}\frac{\rho}{\triangle t^2}\left[u_z{}_{i,k}^{l+1}-2u_z{}_{i,k}^{l}+u_z{}_{i,k}^{l-1}\right] &= \frac{\lambda+2\mu}{\triangle z^2}\left[u_z{}_{i,k+1}^{l+1}-2u_z{}_{i,k}^{l+1}+u_z{}_{i,k-1}^{l+1}\right]\\ &+\frac{\mu}{\triangle x^2}\left[u_z{}_{i+1,k}^{l+1}-2u_z{}_{i,k}^{l+1}+u_z{}_{i-1,k}^{l+1}\right]\\ &+\frac{\lambda+\mu}{4\triangle x\triangle z}\left[u_x{}_{i+1,k+1}^{l+1}-u_x{}_{i+1,k-1}^{l+1}+u_x{}_{i-1,k-1}^{l+1}-u_x{}_{i-1,k+1}^{l+1}\right]\\ &-\frac{\gamma_2}{2\triangle t}\left[3u_z{}_{i,k}^{l+1}-4u_z{}_{i,k}^{l}+u_z{}_{i,k}^{l-1}\right]\\ &+a_2e^{-c_2(t_{l+1})^2}e^{-\kappa(x_i^2+z_k^2)}.\end{aligned} \tag{4.9}$$

$$\begin{aligned}\left(\frac{\rho}{\triangle t^2}+\frac{3\gamma_2}{2\triangle t}+\frac{2(\lambda+2\mu)}{\triangle z^2}+\frac{2\mu}{\triangle x^2}\right)u_z{}_{i,k}^{l+1} &= \left(\frac{2\rho}{\triangle t^2}+\frac{4\gamma_2}{2\triangle t}\right)u_z{}_{i,k}^{l}\\ &-\left(\frac{\rho}{\triangle t^2}+\frac{\gamma_2}{2\triangle t}\right)u_z{}_{i,k}^{l-1}+\frac{\lambda+2\mu}{\triangle z^2}\left[u_z{}_{i,k+1}^{l+1}+u_z{}_{i,k-1}^{l+1}\right]\\ &+\frac{\mu}{\triangle x^2}\left[u_z{}_{i+1,k}^{l+1}+u_z{}_{i-1,k}^{l+1}\right]\\ &+\frac{\lambda+\mu}{4\triangle x\triangle z}\left[u_x{}_{i+1,k+1}^{l+1}-u_x{}_{i+1,k-1}^{l+1}+u_x{}_{i-1,k-1}^{l+1}-u_x{}_{i-1,k+1}^{l+1}\right]\\ &+a_2e^{-c_2(t_{l+1})^2}e^{-\kappa(x_i^2+z_k^2)}.\end{aligned} \tag{4.10}$$

We denoted some of the terms like:

$$\begin{aligned}A_{P2} &= \frac{\rho}{\triangle t^2}+\frac{3\gamma_2}{2\triangle t}+\frac{2(\lambda+2\mu)}{\triangle z^2}+\frac{2\mu}{\triangle x^2}\\ A_{E2} &= A_{W2}=\frac{\mu}{\triangle x^2}\\ A_{N2} &= A_{S2}=\frac{\lambda+2\mu}{\triangle z^2}\\ b2 &= \left(\frac{2\rho}{\triangle t^2}+\frac{4\gamma_2}{2\triangle t}\right)u_z{}_{i,k}^{l}-\left(\frac{\rho}{\triangle t^2}+\frac{\gamma_2}{2\triangle t}\right)u_z{}_{i,k}^{l-1}\\ ACu_x^{l+1} &= \frac{\lambda+\mu}{4\triangle x\triangle z}\left[u_x{}_{i+1,k+1}^{l+1}-u_x{}_{i+1,k-1}^{l+1}+u_x{}_{i-1,k-1}^{l+1}-u_x{}_{i-1,k+1}^{l+1}\right],\end{aligned} \tag{4.11}$$

then, replacing (4.11) in (4.10), we have

$$\begin{aligned}u_z{}_{i,k}^{l+1} = \frac{1}{A_{P2}}\Big[&A_{N2}u_z{}_{i,k+1}^{l+1}+A_{S2}u_z{}_{i,k-1}^{l+1}+A_{E2}u_z{}_{i+1,k}^{l+1}+A_{W2}u_z{}_{i-1,k}^{l+1}+b2+ACu_x^{l+1}+\\ &a_2e^{-c_2(t_{l+1})^2}e^{-\kappa_2(x_i^2+z_k^2)}\Big].\end{aligned} \tag{4.12}$$

Note again that the Equation (4.12) results in an implicit scheme, therefore it results in a system of equations, which is expressed in blocks of tridiagonal matrices. Following the same path we obtain

$$A_2u_z = B_2 \tag{4.13}$$

$$\underbrace{\begin{bmatrix} A_{P2}-A_{N2} & -A_{E2} & & & & & & \\ -A_{S2}A_{P2}-A_{N2} & -A_{E2} & & & & & & \\ \ddots & \ddots & \ddots & \ddots & & & & \\ -A_{S2}A_{P2}-A_{N2} & -A_{E2} & & & & & & \\ -A_{S2}A_{P2} & -A_{E2} & & & & & & \\ \ddots & \ddots & \ddots & \ddots & & & & \\ & & & -A_{W2}A_{P2}-A_{N2} & & & & \\ & & & -A_{W2}-A_{S2}A_{P2}-A_{N2} & & & & \\ & & & \ddots & \ddots & \ddots & \ddots & \\ & & & -A_{W2}-A_{S2}A_{P2}-A_{N2} & & & & \\ & & & -A_{W2} & -A_{S2}A_{P2} & & & \end{bmatrix}}_{A_2} \cdot \underbrace{\begin{bmatrix} u_z{}_{2,2}^{l+1} \\ u_z{}_{2,3}^{l+1} \\ \vdots \\ u_z{}_{2,n-2}^{l+1} \\ u_z{}_{2,n-1}^{l+1} \\ \vdots \\ u_z{}_{n-1,2}^{l+1} \\ u_z{}_{n-1,3}^{l+1} \\ \vdots \\ u_z{}_{n-1,n-2}^{l+1} \\ u_z{}_{n-1,n-1}^{l+1} \end{bmatrix}}_{u_z} =$$

$$= \underbrace{\begin{bmatrix} b2_{2,2}+ACu_x{}_{2,2}^{l+1}+A_{W2}u_z{}_{2,1}^{l+1}+A_{S2}u_z{}_{1,2}^{l+1} \\ b2_{2,3}+ACu_x{}_{2,3}^{l+1}+A_{W2}u_z{}_{1,3}^{l+1} \\ \vdots \\ b2_{2,n-2}+ACu_x{}_{2,n-2}^{l+1}+A_{W2}u_z{}_{1,n-2}^{l+1} \\ b2_{2,n-1}+ACu_x{}_{2,n-1}^{l+1}+A_{W2}u_z{}_{2,n}^{l+1}+A_{N2}u_z{}_{1,n-1}^{l+1} \\ \vdots \\ b2_{n-1,2}+ACu_x{}_{n-1,2}^{l+1}+A_{E2}u_z{}_{n-1,1}^{l+1}+A_{S2}u_z{}_{n,2}^{l+1} \\ b2_{n-1,3}+ACu_x{}_{n-1,3}^{l+1}+A_{E2}u_z{}_{n,3}^{l+1} \\ \vdots \\ b2_{n-1,n-2}+ACu_x{}_{n-1,n-2}^{l+1}+A_{E2}u_z{}_{n,n-2}^{l+1} \\ b2_{n-1,n-1}+ACu_x{}_{n-1,n-1}^{l+1}+A_{E2}u_z{}_{n,n-1}^{l+1}+A_{N2}u_z{}_{n-1,n}^{l+1} \end{bmatrix}}_{B_2}, \tag{4.14}$$

resolving this matrix give us the points $u_z{}_{i,k}^{l+1}$ within the grid, and the other points make up the coefficient matrix B_2.

The equations (4.6) and (4.12) will be resolved with the conditions that will be seen below.

4.3 Discretization of initial and boundary conditions.

The initial conditions given in the equations (3.18) and (3.19), it is easily discretized as,

$$u_{x}{}_{i,k}^{1} = 0 \tag{4.15}$$

$$u_{z}{}_{i,k}^{1} = 0. \tag{4.16}$$

Neumann-type boundary conditions given in the equations (3.16) and (3.17), they are discretized by the method of backward difference as follows:

$$\left.\frac{\partial u_x}{\partial n}\right|_{B1}^{l+1} = \left.\frac{\partial u_x}{\partial n}\right|_{B3}^{l+1} = \frac{u_x|_E^{l+1} - u_x|_W^{l+1}}{\Delta x} = 0$$
$$u_x|_E^{l+1} = u_x|_W^{l+1}\,, \tag{4.17}$$

the same for u_z,

$$\left.\frac{\partial u_z}{\partial n}\right|_{B1}^{l+1} = \left.\frac{\partial u_z}{\partial n}\right|_{B3}^{l+1} = \frac{u_z|_E^{l+1} - u_z|_W^{l+1}}{\Delta x} = 0$$
$$u_z|_E^{l+1} = u_z|_W^{l+1}\,, \tag{4.18}$$

$B2$ and $B4$ to u_x

$$\left.\frac{\partial u_x}{\partial n}\right|_{B2}^{l+1} = \left.\frac{\partial u_x}{\partial n}\right|_{B4}^{l+1} = \frac{u_x|_N^{l+1} - u_x|_S^{l+1}}{\Delta z} = 0$$
$$u_x|_N^{l+1} = u_x|_S^{l+1} \tag{4.19}$$

discretization for $B4$ in u_z is the same,

$$\left.\frac{\partial u_z}{\partial n}\right|_{B4}^{l+1} = \frac{u_z|_N^{l+1} - u_z|_S^{l+1}}{\Delta z} = 0$$
$$u_z|_N^{l+1} = u_z|_S^{l+1} \tag{4.20}$$

except for $B2$, such as

$$\left.\frac{\partial u_z}{\partial n}\right|_{B2}^{l+1} = \frac{u_x|_N^{l+1} - u_x|_S^{l+1}}{\Delta z} = \dot{Q}$$
$$u_z|_N^{l+1} = \dot{Q}\Delta z + u_z|_S^{l+1}\,, \tag{4.21}$$

where $\dot{Q}$ is the parameter of rate of variation of the wave near the surface.

4.4 STABILITY AND CONSISTENCY OF THE DISCRETIZED MODEL

In the context of discretization of partial differential equations, it is known that smaller values of Δx and Δz lead to an increase in the number of calculations performed for a fixed point (x; z). This can lead to an accumulation of errors, which lead to instability. For implicit discretization schemes, stability is guaranteed (CUMINATO; MENEGUETTE, 2013).

The finite difference representation of a partial differential equation is said to be consistent if the finite difference equation approaches the partial derivative equation by decreasing the size of the interval $\Delta x,\ \Delta z$ and Δt as mentioned in the following definition:

Definition 4.1. *Given a differential equation $Pu = f$ and a finite difference scheme $P_{h,k}u = f$; we say that the finite difference equation is consistent with the partial differential equation (EDP) if and only if for any smooth function $\phi(x,t)$, it is true that,*

$$P\phi - P_{h,k}\phi \ \rightarrow \ 0 \textit{ when } h,k \ \rightarrow \ 0,$$

where the convergence is punctual, this means at each point of the mesh.

The equations P-SV given by (3.13) and (3.14)

$$\frac{\partial^2 u_x}{\partial t^2} + \gamma_1 \frac{\partial u_x}{\partial t} = \frac{\lambda + 2\mu}{\rho}\left(\frac{\partial^2 u_x}{\partial x^2} + \frac{\partial^2 u_z}{\partial z \partial x}\right) + \frac{\mu}{\rho}\left(\frac{\partial^2 u_x}{\partial z^2} - \frac{\partial^2 u_z}{\partial z \partial x}\right) \tag{4.22}$$

$$\frac{\partial^2 u_z}{\partial t^2} + \gamma_2 \frac{\partial u_z}{\partial t} = \frac{\lambda + 2\mu}{\rho}\left(\frac{\partial^2 u_x}{\partial x \partial z} + \frac{\partial^2 u_z}{\partial z^2}\right) + \frac{\mu}{\rho}\left(\frac{\partial^2 u_z}{\partial x^2} - \frac{\partial^2 u_x}{\partial x \partial z}\right). \tag{4.23}$$

Denoting by

$$\begin{aligned} \beta^2 = \frac{\mu}{\rho} \ \rightarrow \ \beta = \sqrt{\frac{\mu}{\rho}} \\ \alpha^2 = \frac{\lambda + 2\mu}{\rho} \ \rightarrow \ \alpha = \sqrt{\frac{\lambda + 2\mu}{\rho}} \end{aligned} \tag{4.24}$$

Changing the notation to summarize the equation (4.22) and (4.23), we obtain the following matricial differential equation

$$U_{tt} + \gamma U_t = AU_{xx} + BU_{xz} + CU_{zz}, \tag{4.25}$$

where

$$U = \begin{pmatrix} u_x \\ u_z \end{pmatrix} \quad \gamma = \begin{pmatrix} \gamma_1 & 0 \\ 0 & \gamma_2 \end{pmatrix} \quad A = \begin{pmatrix} \alpha^2 & 0 \\ 0 & \beta^2 \end{pmatrix} \quad B = \begin{pmatrix} 0 & \alpha^2 - \beta^2 \\ \alpha^2 - \beta^2 & 0 \end{pmatrix} \quad C = \begin{pmatrix} \beta^2 & 0 \\ 0 & \alpha^2 \end{pmatrix}.$$

in a simpler way for the consistency analysis.

Let P be an auxiliary variable and ϕ a smooth function, so that

$$P\phi = A\phi_{xx} + B\phi_{xz} + C\phi_{zz} - \phi_{tt} - \gamma\phi_t. \tag{4.26}$$

Discretizing the equation (4.25) using central differences for spacial derivatives and the terms of second derivative and backward second order difference for temporal derivatives, we have

$$
\begin{aligned}
P_{\Delta x,\Delta z,\Delta t}\phi = A&\left(\frac{\phi^{l+1}_{i+1,k}-2\phi^{l+1}_{i,k}+\phi^{l+1}_{i-1,k}}{\Delta x^2}\right)+B\left(\frac{\phi^{l+1}_{i+1,k+1}-\phi^{l+1}_{i+1,k-1}+\phi^{l+1}_{i-1,k-1}-\phi^{l+1}_{i-1,k+1}}{4\Delta x\Delta z}\right)\\
&+C\left(\frac{\phi^{l+1}_{i,k+1}-2\phi^{l+1}_{i,k}+\phi^{l+1}_{i,k-1}}{\Delta z^2}\right)-\left(\frac{\phi^{l+1}_{i,k}-2\phi^{l}_{i,k}+\phi^{l-1}_{i,k}}{\Delta t^2}\right)\\
&-\gamma\left(\frac{3\phi^{l+1}_{i,k}-4\phi^{l}_{i,k}+\phi^{l-1}_{i,k}}{2\Delta t}\right)
\end{aligned}
\tag{4.27}
$$

where,

$$
\phi^{l+1}_{i,k}=\phi(i,k,l). \tag{4.28}
$$

To obtain (4.27), we use the Taylor expansion for each term in that equation, namely,

$$
\begin{aligned}
\phi^{l+1}_{i+1,k}&=\phi^{l+1}_{i,k}+\Delta x\phi_x+\frac{1}{2}\Delta x^2\phi_{xx}+O(\Delta x^3)\\
\phi^{l+1}_{i-1,k}&=\phi^{l+1}_{i,k}-\Delta x\phi_x+\frac{1}{2}\Delta x^2\phi_{xx}+O(\Delta x^3)\\
\phi^{l+1}_{i,k+1}&=\phi^{l+1}_{i,k}+\Delta z\phi_z+\frac{1}{2}\Delta z^2\phi_{zz}+O(\Delta z^3)\\
\phi^{l+1}_{i,k-1}&=\phi^{l+1}_{i,k}-\Delta z\phi_z+\frac{1}{2}\Delta z^2\phi_{zz}+O(\Delta z^3)\\
\phi^{l+1}_{i,k}&=\phi^{l}_{i,k}+\Delta t\phi_t+\frac{1}{2}\Delta t^2\phi_{tt}+O(\Delta t^3)\\
\phi^{l-1}_{i,k}&=\phi^{l}_{i,k}-\Delta t\phi_t+\frac{1}{2}\Delta t^2\phi_{tt}+O(\Delta t^3)\\
\phi^{l+1}_{i+1,k+1}&=\phi^{l+1}_{i,k}+\Delta x\phi_x+\Delta z\phi_z+\frac{1}{2}\Delta x^2\phi_{xx}+\frac{1}{2}\Delta z^2\phi_{zz}+\Delta x\Delta z\phi_{xz}+O\left[(\Delta x^3,\Delta z^3)\right]\\
\phi^{l+1}_{i-1,k-1}&=\phi^{l+1}_{i,k}-\Delta x\phi_x-\Delta z\phi_z+\frac{1}{2}\Delta x^2\phi_{xx}+\frac{1}{2}\Delta z^2\phi_{zz}+\Delta x\Delta z\phi_{xz}+O\left[(\Delta x^3,\Delta z^3)\right]\\
\phi^{l+1}_{i+1,k-1}&=\phi^{l+1}_{i,k}+\Delta x\phi_x-\Delta z\phi_z+\frac{1}{2}\Delta x^2\phi_{xx}+\frac{1}{2}\Delta z^2\phi_{zz}-\Delta x\Delta z\phi_{xz}+O\left[(\Delta x^3,\Delta z^3)\right]\\
\phi^{l+1}_{i-1,k+1}&=\phi^{l+1}_{i,k}-\Delta x\phi_x+\Delta z\phi_z+\frac{1}{2}\Delta x^2\phi_{xx}+\frac{1}{2}\Delta z^2\phi_{zz}-\Delta x\Delta z\phi_{xz}+O\left[(\Delta x^3,\Delta z^3)\right].
\end{aligned}
\tag{4.29}
$$

From the equations in (4.27), we obtain that

$$
\begin{aligned}
\left(\frac{\Phi_{i+1,k}^{l+1}-2\Phi_{i,k}^{l+1}+\Phi_{i-1,k}^{l+1}}{\Delta x^2}\right) &= \Phi_{xx}+O(\Delta x^2)\\
\left(\frac{\Phi_{i+1,k+1}^{l+1}-\Phi_{i+1,k-1}^{l+1}+\Phi_{i-1,k-1}^{l+1}-\Phi_{i-1,k+1}^{l+1}}{4\Delta x\Delta z}\right) &= \Phi_{xz}+O\left[(\Delta x^2,\Delta z^2)\right]\\
\left(\frac{\Phi_{i,k+1}^{l+1}-2\Phi_{i,k}^{l+1}+\Phi_{i,k-1}^{l+1}}{\Delta z^2}\right) &= \Phi_{zz}+O(\Delta z^2)\\
\left(\frac{\Phi_{i,k}^{l+1}-2\Phi_{i,k}^{l}+\Phi_{i,k}^{l-1}}{\Delta t^2}\right) &= \Phi_{tt}+O(\Delta t^2)\\
\left(\frac{3\Phi_{i,k}^{l+1}-4\Phi_{i,k}^{l}+\Phi_{i,k}^{l-1}}{2\Delta t}\right) &= \Phi_{t}+\Delta t\Phi_{tt}+\frac{1}{6}\Delta t^2\Phi_{ttt}+O(\Delta t^2).
\end{aligned}
\tag{4.30}
$$

Applying Definition 4.1 thus, substituting (4.30) in (4.27) and subtracting this result from (4.26), we have

$$
\begin{aligned}
P\phi = {} & \gamma\Delta t\phi_{tt}+\frac{1}{6}\Delta t^2\phi_{ttt}+\gamma O(\Delta t^2)+O(\Delta x^2)+O(\Delta z^2)\\
& -O(\Delta t^2)+O\left[(\Delta x^2,\Delta z^2)\right],
\end{aligned}
\tag{4.31}
$$

and then taking the limit.

$$
\lim_{\Delta x,\Delta z,\Delta t\to 0}\left[P_{\Delta x,\Delta z,\Delta t}\Phi-P\Phi\right]=0, \tag{4.32}
$$

which demonstrates the consistency of the discretization of the differential equations.

Definition 4.2. *A method based on finite differences is convergent if and only if it is stable and consistent.*

According to the previous definition, it serves as an indicator to say that our implicit scheme given by finite differences is convergent.

4.5 Computational Algorithm Structure.

Next, we present the structure of the computational algorithm used in this numerical model.

ALGORITHM STRUCTURE FOR u_x, AND u_z USING GAUSS SAIDEL (OCTAVE)

INPUT: EARTHQUAKE'S HYPOCENTER, z_0, z_f, x_0, x_f, t_f, MT, ρ, α, β, μ, λ, $\gamma_{1,2}$, $a_{1,2}$, $c_{1,2}$, $\kappa_{1,2}$, ITMAX, TOLERANCE, NZ, and NX.

OUTPUT: u_x, u_z, and $\sqrt{u_x^2 + u_z^2}$

Step 1, run GRID.M

Step 2, run INITIAL CONDITIONS.M given in the equations (4.15), and (4.16).

Create a file to save the simulation images at each time.

FRAME = 0

Step 3, run OUTPUT.M

Step 4, $U_{xA} = U_x$, $U_{xAA} = U_x$, $U_{xN} = U_x$, $U_{zA} = U_z$, $U_{zAA} = U_z$, and $U_{zN} = U_z$

Step 5,

WHILE $t < t_f$

FRAME = FRAME + 1

FOR IT: 1: ITMAX

run EQUATION U_x.M and EQUATION U_z.M given by the equation (4.6) and (4.12).

run BOUNDARY CONDITIONS.M given by the equations (4.17), (4.18), (4.19), (4.20), and (4.21).

We use the 1-norm, or largest column sum of $U_{xN} - U_x$, to measure the error for each iteration, this is;

NORM U_x = NORM $(U_{xN} - U_x, 1)$/ NORM $(U_{xN}, 1)$

NORM U_z = NORM $(U_{xN} - U_z, 1)$/ NORM $(U_{zN}, 1)$

NORM MAX = MAX ([NORM U_x, NORM U_z])

$U_x = U_{xN}$, $U_z = U_{zN}$

IF (NORM MAX $<$ TOLERANCE)

$U_{xAA} = U_{xA}$, $U_{xA} = U_x$, $U_{zAA} = U_{zA}$, and $U_{zA} = U_z$

run OUTPUT.M

Do $t + dt$, and break when it converges to a number less than tolerance.

BREAK

ELSE IT = ITMAX, which means that the solution does not converge and reached the maximum iteration.

END IF

END FOR

END WHILE

5 RESULTS

In this chapter we present the numerical simulations carried out from the constructed mathematical and numerical models.

5.1 DYNAMICS OF A PERFECT WAVE.

In this section we present and discuss simulations for a P-SV wave equations given by (3.13), and (3.14) equations, with $\lambda = -\mu$. In this case, the shear forces and pressure forces are equal and the wave is described by decoupled perfect wave equations, when attenuation and source forces are avoided. Substituting $\lambda = -\mu$ into (3.13), and (3.14), we get

$$\rho \frac{\partial^2 u_x}{\partial t^2}\Big|_{i,k}^{l+1} = \mu \frac{\partial^2 u_x}{\partial x^2}\Big|_{i,k}^{l+1} + \mu \frac{\partial^2 u_x}{\partial z^2}\Big|_{i,k}^{l+1} - \gamma_1 \frac{\partial u_x}{\partial t}\Big|_{i,k}^{l+1} + E_x\Big|_{i,k}^{l+1} \tag{5.1}$$

$$\rho \frac{\partial^2 u_z}{\partial t^2}\Big|_{i,k}^{l+1} = \mu \frac{\partial^2 u_z}{\partial z^2}\Big|_{i,k}^{l+1} + \mu \frac{\partial^2 u_z}{\partial x^2}\Big|_{i,k}^{l+1} - \gamma_2 \frac{\partial u_z}{\partial t}\Big|_{i,k}^{l+1} + E_z\Big|_{i,k}^{l+1}. \tag{5.2}$$

Next, we will do several numerical simulations to understand the influence of the parameters of the mathematical model on the evolution of the variables u_x and u_z.

5.1.1 Study of $\kappa_{1,2}$ parameters

The source's parameters κ_1 and κ_2 effect on the behavior of the displacement equations, because they represent the spatial distribution of the source force in the x and z directions, respectively. To obtain simulations due only to the variation of $\kappa_{1,2}$, we are going to set the other parameters as $\rho = 1$ Kg/m^3, $\mu = 1$ Kg/m s^2, $c_{1,2} = 1$ s$^-$2=Hz^2, $a_{1,2} = 1$N, and $\gamma_{1,2} = 0$ Kg/s m^3 . In all simulated cases, we present the results for u_x, u_z, and $u = \sqrt{u_x^2 + u_x^2}$.

In Figures (5.1), (5.2), and (5.3) show P-SV waves affected by variations in κ. Figures (5.1), and (5.2) with $\kappa_1 > 0.1\text{m}^{-2}$ the wave is less intense, almost zero in u_x, while for $\kappa_2 = 0.1$ m^{-2} the intensity of the wave is greater in u_z. In Figure (5.3), we use $\kappa_{1,2} = 0.1$ m^{-2} obtaining a more intense wave with respect to Figures (5.1), and (5.2) for u. The values $\kappa_{1,2} = 0.1$ m^{-2} are considered adequate for our model, and they will be used for the following simulations.

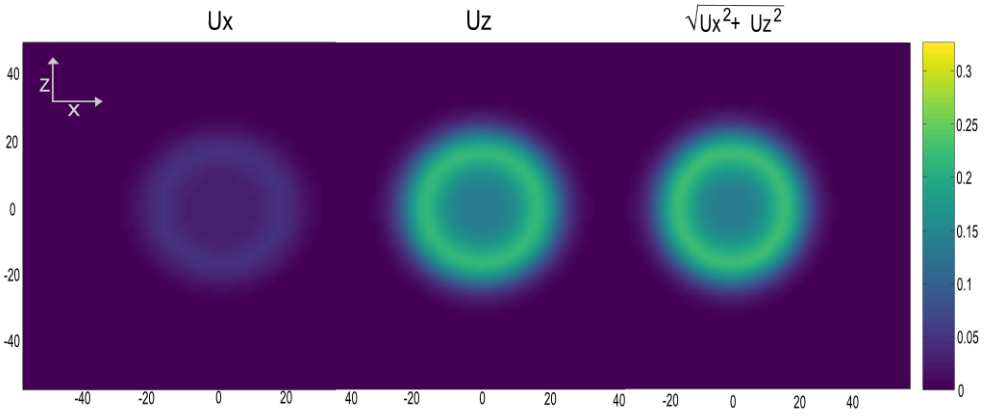

Figure 5.1: Simulation of horizontal and vertical displacement with $\kappa_1 = 0.5$ m^{-2} for u_x, and $\kappa_2 = 0.1$ m^{-2} for u_z. The influence of κ_2 is greater in u, with $\gamma_{1,2} = 0$ Kg/s m^3, and $c_{1,2} = 1$ Hz^2

Source: Author

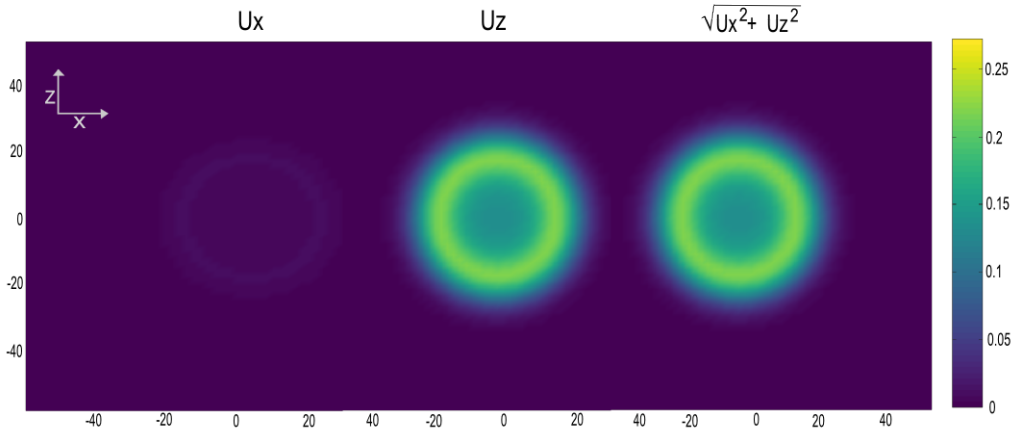

Figure 5.2: Simulation of horizontal and vertical displacement with $\kappa_1 = 10$ m^{-2} for u_x, and $\kappa_2 = 0.1$ m^{-2} for u_z. The influence of κ_1 is less for u, with $\gamma_{1,2} = 0$Kg/s m^3, and $c_{1,2} = 1$Hz^2

Source: Author

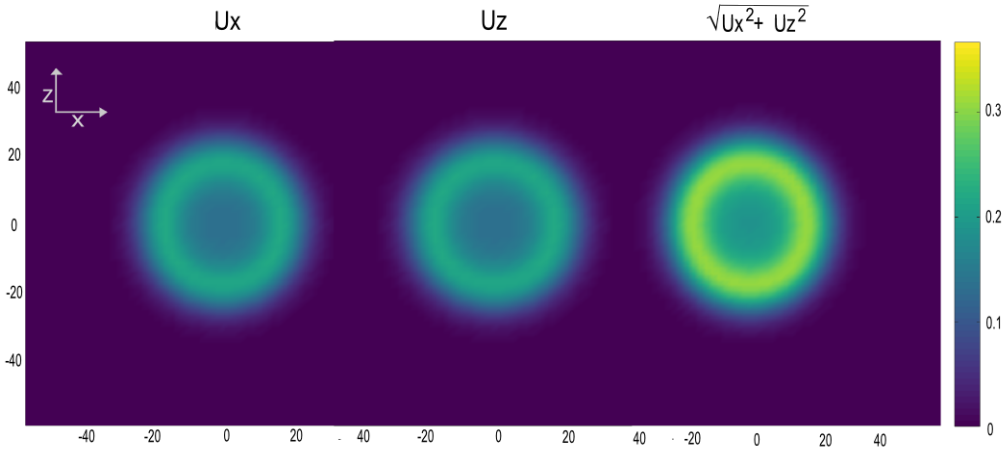

Figure 5.3: Simulation of horizontal and vertical displacement with $\kappa_1 = 0.1\text{m}^{-2}$ for u_x, and $\kappa_2 = 0.1\text{m}^{-2}$ for u_z. The influence of κ_1 is the same for u, with $\gamma_{1,2} = 0\text{Kg/s m}^3$, and $c_{1,2} = 1\text{Hz}^2$

Source: Author

5.1.2 Study of $c_{1,2}$ parameters

The parameters c represent the temporal distribution of the source force in the x and z directions, respectively. They can also simulate the frequency of the source (BAI et al., 2013). For the study of this parameters we are going to set the parameters $\rho = 1$ Kg/m^3, $\mu = 1\text{Kg/m s}^2$, $a_{1,2} = 1\text{N}$, $\kappa_{1,2} = 0.1\text{m}^{-2}$ and, $\gamma_{1,2} = 0\text{Kg/s m}^3$. The results are shown for u_x, u_z, and $u = \sqrt{u_x^2 + u_x^2}$, when only $c_{1,2}$ changes.

In Figure (5.4) shows the intensity of the wave, which is less when $c_{1,2} > 1$ for u_x, and u_z compared to Figure (5.5), where $c_{1,2} = 0.1\text{Hz}^2$.

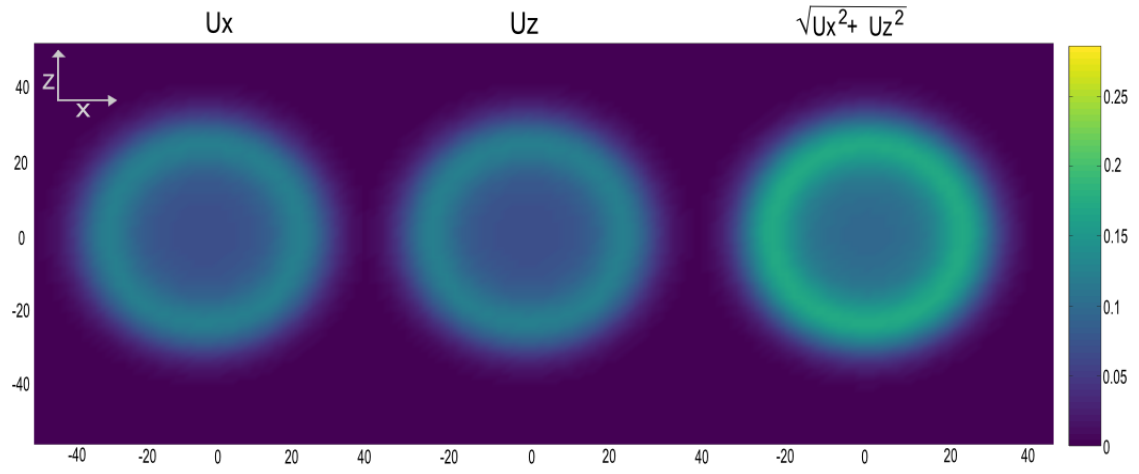

Figure 5.4: Simulation of horizontal and vertical displacement for a Wave without attenuation $\gamma_{1,2} = 0$Kg/s m^3 with $\kappa_{1,2} = 0.1\text{m}^{-2}$, and $c_{1,2} = 1.5\text{Hz}^2$
Source: Author

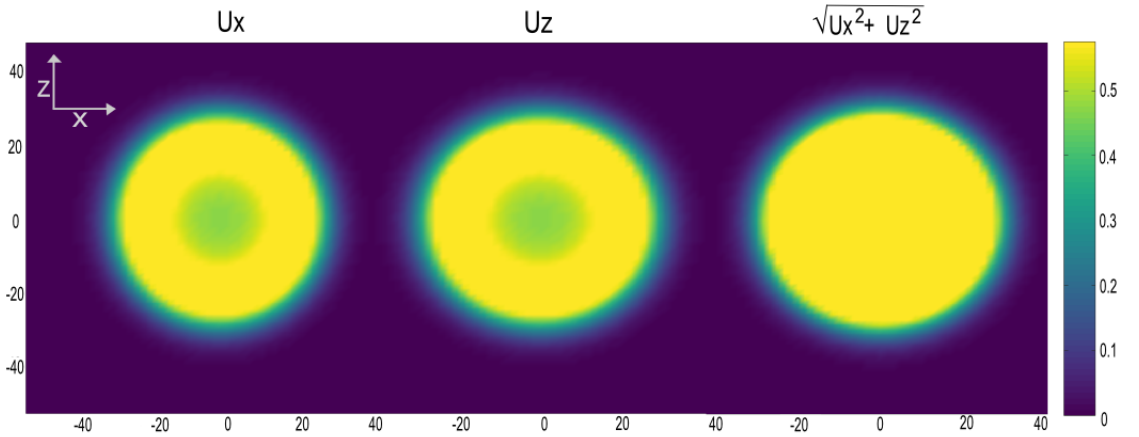

Figure 5.5: Simulation of horizontal and vertical displacement for a Wave without attenuation $\gamma_{1,2} = 0$Kg/s m^3 with $\kappa_{1,2} = 0.1\text{m}^{-2}$, and $c_{1,2} = 0.1\text{Hz}^2$
Source: Author

5.1.3 Study of the $\gamma_{1,2}$ parameters

The parameter $\gamma_{1,2}$ allows to simulate the wave in a medium with attenuation forces. For the study of these parameters, the values for the other parameters are taken as $\rho = 1$ Kg/m^3, $\mu = 1$Kg/m s^2, $a_{1,2} = 1$N, $\kappa_{1,2} = 0.1\text{m}^{-2}$ and, $c_{1,2} = 0.1\text{Hz}^2$. The results are displayed for u_x, u_z, and $u = \sqrt{u_x^2 + u_x^2}$ changing $\gamma_{1,2}$

In figure (5.6), it shows the wave being noticeably more attenuated at u_x, and u_z when $\gamma_{1,2} = 0.1$ Kg/s m^3, however in Figure (5.7), using $\gamma_1 = 0.01$ Kg/s m^3, and $\gamma_2 = 0.1$ Kg/s m^3, shows the attenuation intensity, which is less in u_x compared to u_z. In Figure (5.8), using $\gamma_{1,2} = 0.01$ Kg/s m^3, we observe that the waves are slightly attenuated, resulting in u more intense compared to Figure (5.7) for u.

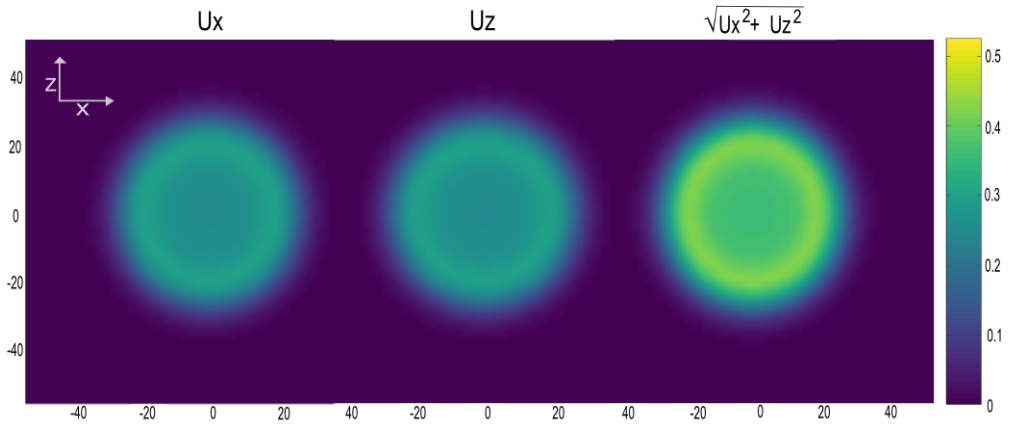

Figure 5.6: Simulation of horizontal and vertical displacement for a wave with attenuation $\gamma_{1,2} = 0.1$ Kg/s m^3 , $\kappa_{1,2} = 0.1\text{m}^{-2}$, and $c_{1,2} = 0.1\text{Hz}^2$
Source: Author

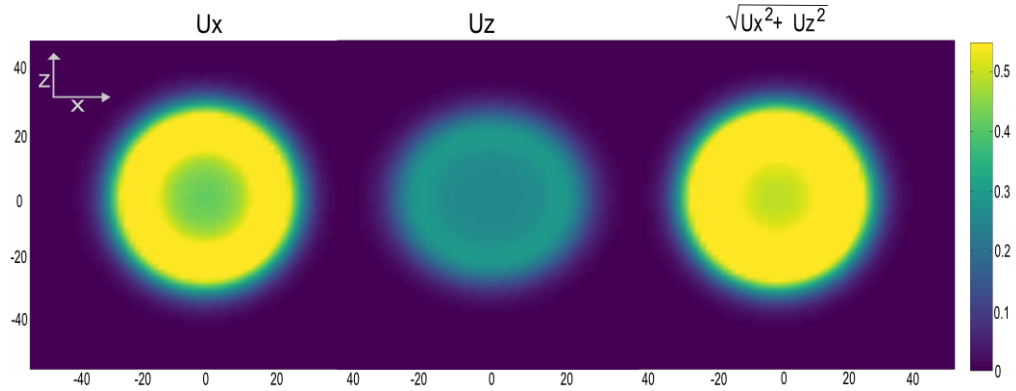

Figure 5.7: Simulation of horizontal and vertical displacement for a wave with attenuation $\gamma_1 = 0.01$ Kg/s m^3, and $\gamma_2 = 0.1$ Kg/s m^3, with $\kappa_{1,2} = 0.1\text{m}^{-2}$, and $c_{1,2} = 0.1\text{Hz}^2$
Source: Author

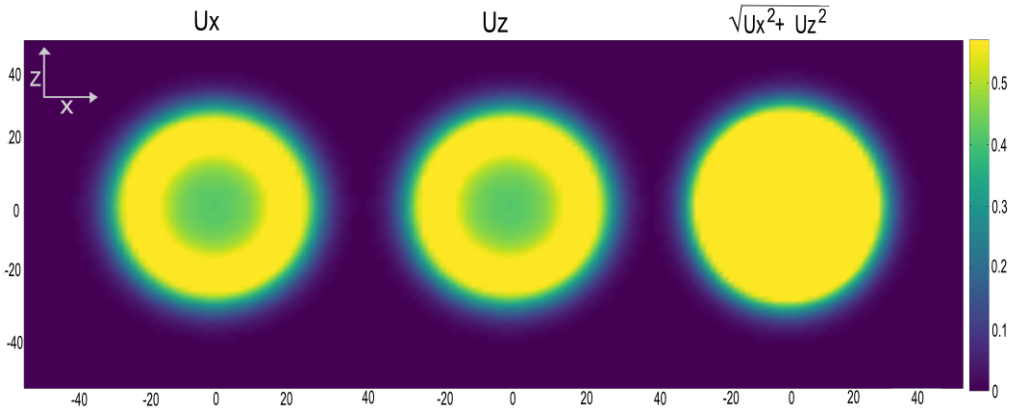

Figure 5.8: Simulation of horizontal and vertical displacement for a wave with attenuation $\gamma_{1,2} = 0.01$ Kg/s m^3, with $\kappa_{1,2} = 0.1\text{m}^{-2}$, and $c_{1,2} = 0.1\text{Hz}^2$
Source: Author

According to the previous studies we can say that the numerical model is being sensitive to the parameters for the source and attenuation. In the next section we are going to use physical values for the model parameters, which refers to the physical properties of the medium.

5.2 DYNAMICS OF THE P-SV SEISMIC WAVES WITH REAL PARAMETERS.

In this section we are going to use real values available in the literature, especially parameters that represent the propagation speed α, and β for P, and S waves, respectively. Velocity parameters are more used in literature for the simulation of seismic waves in different media. The use of elastic parameters λ , and μ is less common.

So, setting the P-speed as α and the SV-speed as β, from equation (4.24) we have

$$\alpha = \sqrt{\frac{\lambda + 2\mu}{\rho}} \qquad\qquad \beta = \sqrt{\frac{\mu}{\rho}}$$

and then rewriting the P-SV discretized wave equations in terms of these velocities, we get

$$\frac{\partial^2 u_x}{\partial t^2}\Big|_{i,k}^{l+1} = \alpha^2 \frac{\partial^2 u_x}{\partial x^2}\Big|_{i,k}^{l+1} + \beta^2 \frac{\partial^2 u_x}{\partial z^2}\Big|_{i,k}^{l+1} + (\alpha^2 - \beta^2)\frac{\partial^2 u_z}{\partial z \partial x}\Big|_{i,k}^{l+1} - \gamma_1 \frac{\partial u_x}{\partial t}\Big|_{i,k}^{l+1} + E_x\Big|_{i,k}^{l+1} \tag{5.3}$$

$$\frac{\partial^2 u_z}{\partial t^2}\Big|_{i,k}^{l+1} = \alpha^2 \frac{\partial^2 u_z}{\partial z^2}\Big|_{i,k}^{l+1} + \beta^2 \frac{\partial^2 u_z}{\partial x^2}\Big|_{i,k}^{l+1} + (\alpha^2 - \beta^2)\frac{\partial^2 u_x}{\partial x \partial z}\Big|_{i,k}^{l+1} - \gamma_2 \frac{\partial u_z}{\partial t}\Big|_{i,k}^{l+1} + E_z\Big|_{i,k}^{l+1}. \tag{5.4}$$

Note that to have perfect waves we must use $\alpha = \beta$ in Equations $(5.3 - 5.4)$. For the following simulation we are going to use the parameters of Bai et al. (2013). The first simulation displayed in Figure 5.9, we used a domain of 21000m $\times$ 20500m, cell size $201m \times 172$m and $\alpha = \beta = 1800$m/s. The time interval is 0.01s. Source parameters given by $c_{1,2} = 25\text{Hz}^2$, $a_{1,2} = 10^9$N and $\kappa_{1,2} = 0.1\text{m}^{-2}$. We emphasize that 1 ton of TNT = 4.2×10^9 N m.

For the second simulation, showed in Figure 5.10, we use the same dimension as, 21000m$\times$20500m, and cell size 201m$\times$172m. Velocities $\alpha = 3000$m/s and $\beta = 1800$m/s. The time interval is $0.005 = 5$ ms. Source parameters given by $c_{1,2} = 25\text{Hz}^2$, $a_{1,2} = 10^9$N and $\kappa_{1,2} = 0.1\text{m}^{-2}$.

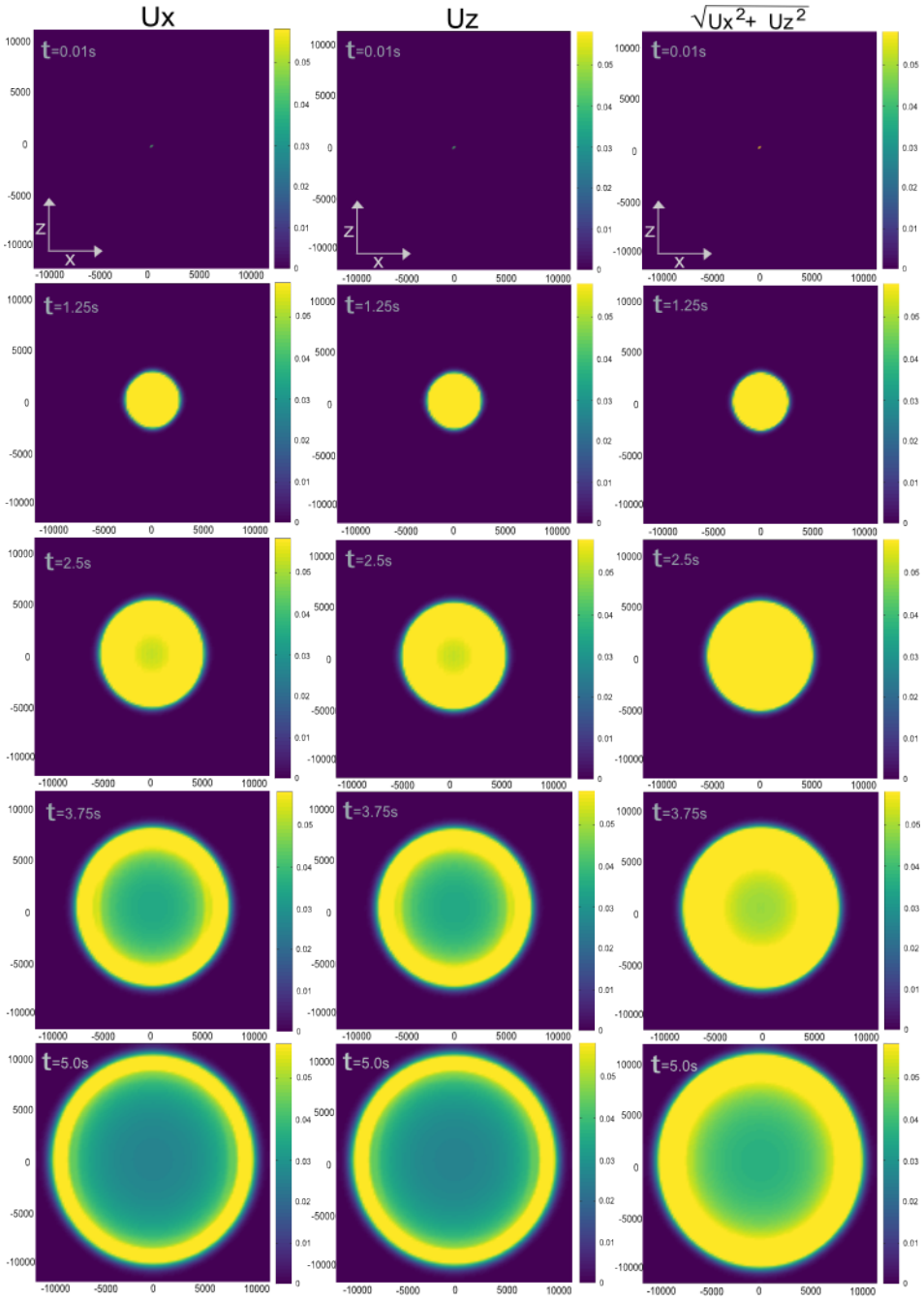

Figure 5.9: The figure shows the effect of the source on u_x, u_z, which is not being attenuated, for velocity $\alpha = \beta = 1800$m/s. The source takes the maximum value for $t = 0.01$s. When the time increases to $t_f = 5$s, the wave moves in the domain 21000m $\times$20500m by the equations $(5.3 - 5.4)$. The time interval is 0.01s. Source parameters given by $c_{1,2} = 25\text{Hz}^2$, $a_{1,2} = 10^9\text{N}$ and $\kappa_{1,2} = 0.1\text{m}^{-2}$.

Source: Author

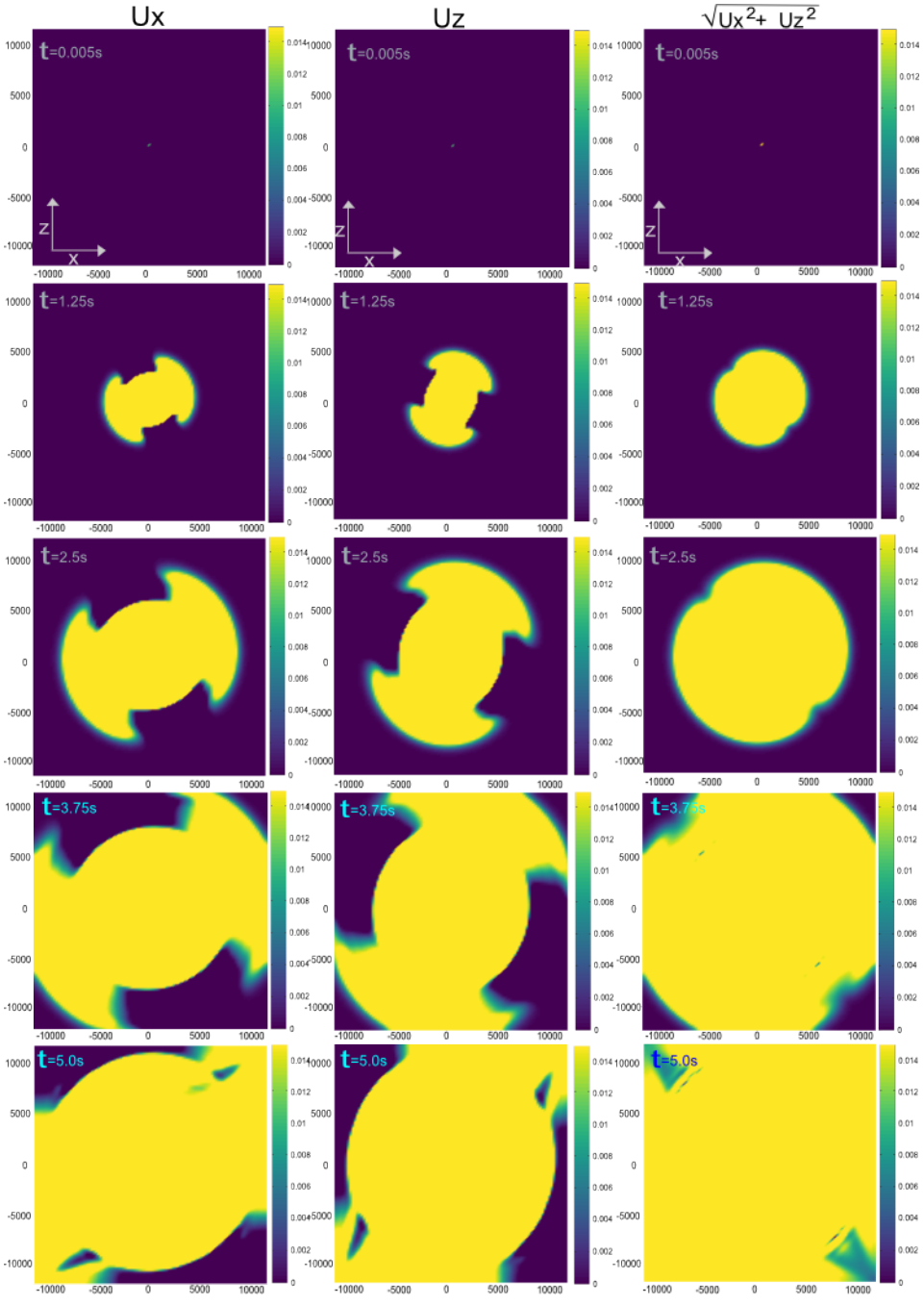

Figure 5.10: The figure shows the effect of the source on u_x, and u_z, which is not being attenuated, for velocity $\alpha = 3000$m/s and $\beta = 1800$m/s. In the time $t = 0.005$s the source takes the maximum at zero, the domain is $21000\text{m}\times 20500\text{m}$. Source parameters given by $c_{1,2} = 25\text{Hz}^2$, $a_{1,2} = 10^9\text{N}$ and $\kappa_{1,2} = 0.1\text{m}^{-2}$

Source: Author

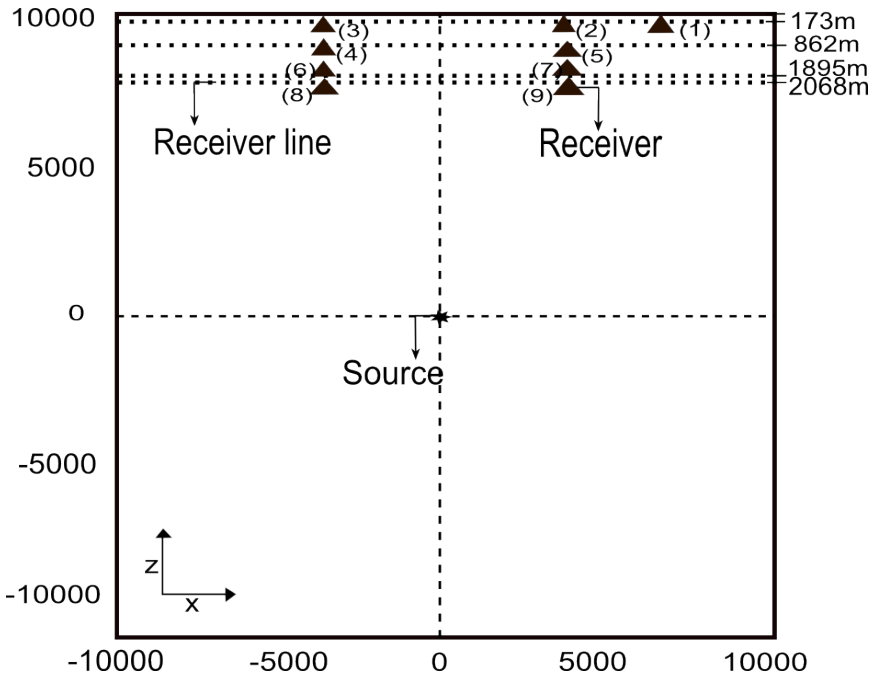

Figure 5.11: Position of 9 seismic wave receivers for seismogram acquisition.

Note that figure 5.9 simulates the propagation of P-SV seismic waves when the propagation velocities of these waves are equal. This situation is unrealistic. In this case we have a perfect wave, with circular symmetry (2D) in its evolution. Note that at $t = 5$, the source (force at the epicenter) has already significantly decreased its intensity.

On the other hand, figure 5.10 actually simulates the propagation of P-SV seismic waves, with model parameters being calibrated to the characteristics of the Brazilian territory. Due to the different speeds of the P and SV waves, a complex interaction of pressure and shear forces in the propagation of these waves is observed. Note that at $t = 3.75$s the waves have already passed through the borders (Newman-type boundary condition) and the horizontal and vertical displacements at a point on the surface (upper border of the domain), over time, generate theoretical seismograms. Such seismograms can be compared with observed seismograms, and thus the depth and location of the epicenter of a given earthquake can be estimated.

5.3 SEISMOGRAMS

The receivers (1-9) in figure 5.11 are located close to the surface. The receivers generate the seismograms for the horizontal and vertical displacements that contain the P-SV waves. The seismograms represent the P-SV waves plotted for u_x and u_z, demonstrating the amplitude of the displacements.

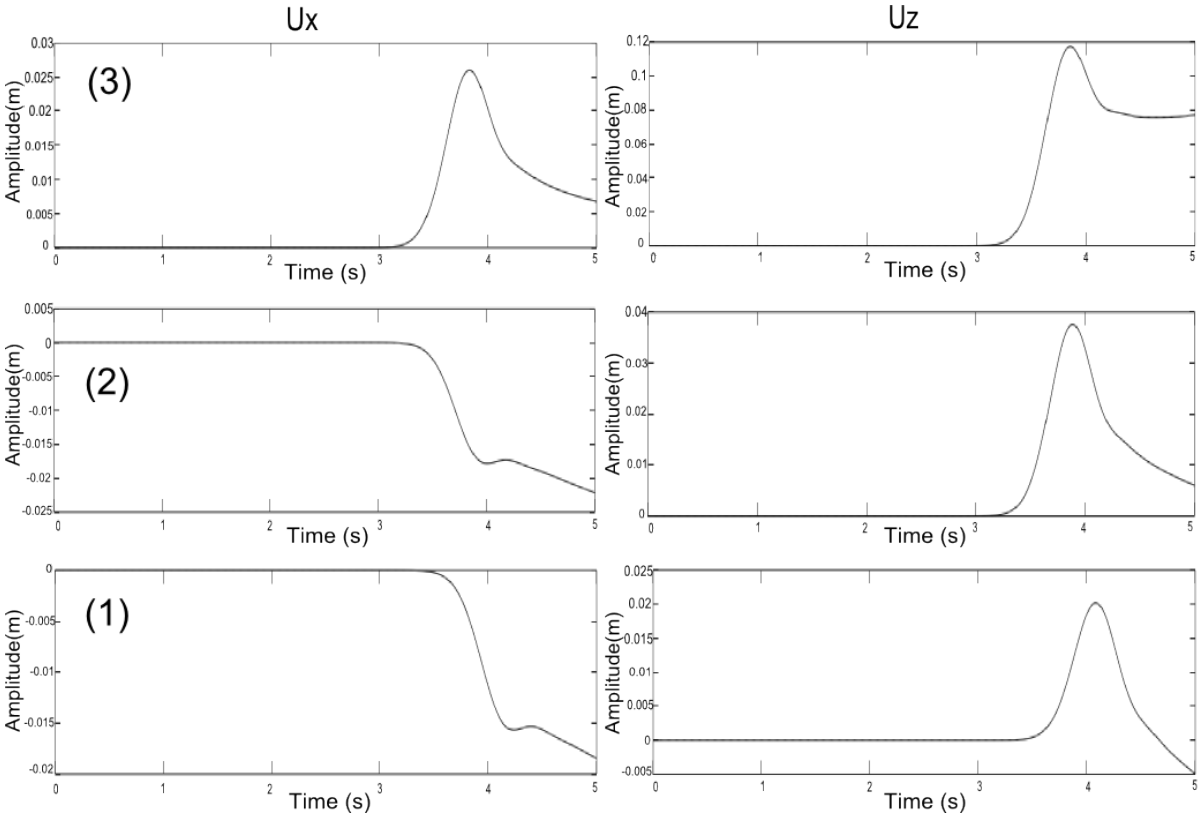

Figure 5.12: Records of(3), (2) and (1) receivers.

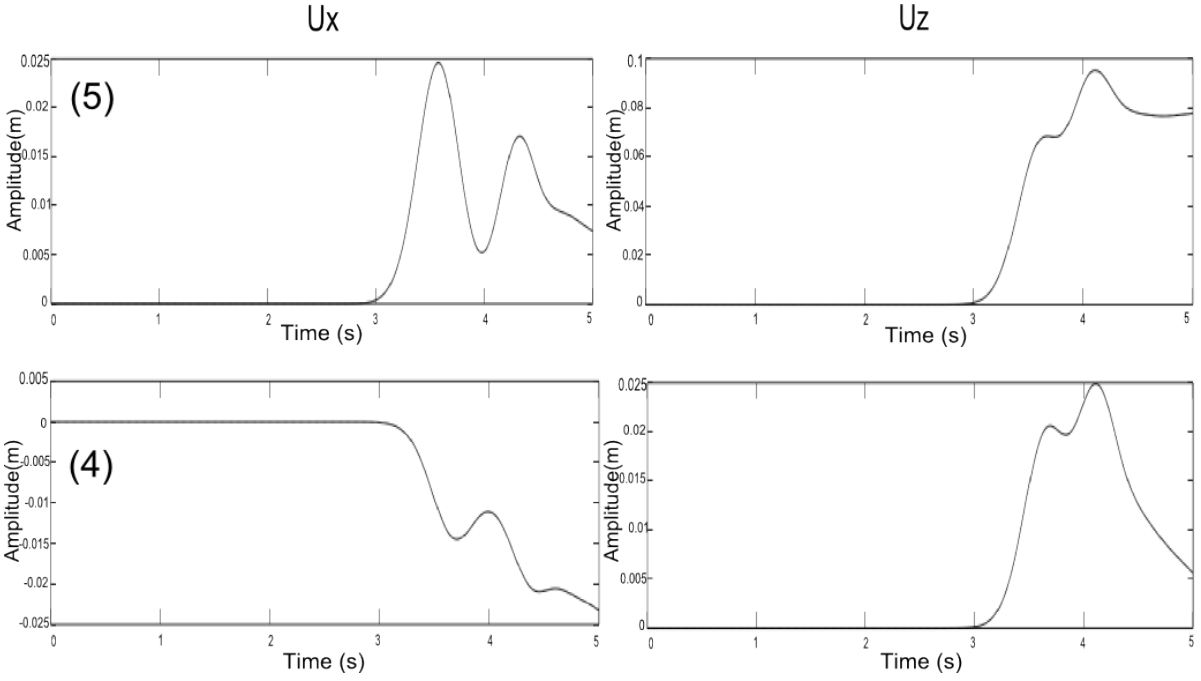

Figure 5.13: Records of(5) and (4) receivers.

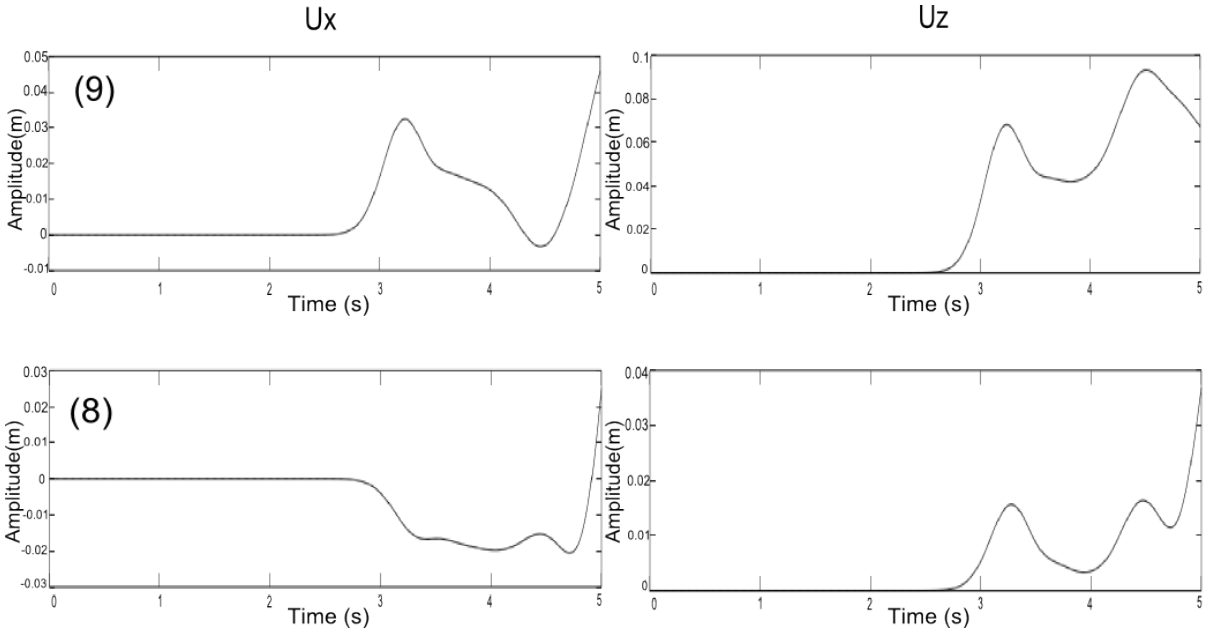

Figure 5.14: Records of(9) and (8) receivers

In the presented seismograms, we noticed that depending on the position and depth of the seismic wave receivers, the seismic waves arrive at different times and with different amplitudes. Note also that for the chosen parameters, the Δx shifts have greater amplitudes than the Δz shifts.

6 CONCLUSIONS

The P-SV wave equations given by (3.13-3.14) represent the displacements that occur in the x and z directions, where the compression P waves have a higher speed compared to the shear SV waves.

We have shown that Brazil has earthquakes of less intensity because it is within the South American plate and not at the border of it, where earthquakes are of great magnitude. The earthquakes that occur at the borders of the South American plate are greater than 50km deep, however, within the plate, fracture earthquakes occur, on average, at a depth of less than 50 km (Centro de Sismologia, USP, 2021). In the simulations presented in this work, the location of the earthquake sources are positioned at depths of 50Km (section 5.1) and 10Km (section 5.2). Such earthquakes are called superficial. Earthquakes that take place at this depth occur in Zones 4, Zone 3, and Zone 2 (SANTOS et al., 2008).

We also consider a magnitude on the Richter scale (Ms) of 3Ms (ASSUMPÇÃO; NETO, 2000), leading us to consider a force for the source of $a_{1,2} = 4.2 \times 10^9$Nm, producing a displacement greater than 1mm. The displacements are shown in Figure 5.10. This can be considered a small magnitude, but the intensity of an earthquake is qualitative, being sometimes devastating for a small magnitude. Observe that there is no direct relationship between magnitude and intensity. The perception of this is measured with the Mercalli scale (Table 2.1).

The disturbance of seismic waves when they propagate through an elastic medium is in the frequency range of 1 to 100 Hertz. We consider 25 Hertz similar to Vierux (1986). On the propagation velocities of the P-SV seismic waves, we use the values of Bai et al. (2013). Note that for clay, depending on its properties and the amount of water, wave propagation speeds range from 1800 m/s to 4800 m/s (NERY, 1990).

For an isotropic medium, the simulations were presented in sections 5.1 and 5.2. In section 5.1 we made a study of the effects of the parameters of the mathematical model on the propagation of the P-SV seismic waves. In section 5.2 we simulate the propagation of these waves in clays to epicenters with a depth of around 10 km.

As possible future work, we intend to extend the results to non-homogeneous media. For example, to study the effect of different layers of the Earth's crust on the propagation of P-SV seismic waves. The earth's crust is basically composed of aluminum silicates (clays), but it also has discontinuities, reservoirs, etc. These inhomogeneities better explain the chaotic behavior of the horizontal and vertical displacements observed in seismograms.

REFERENCES

Alterman, Z. & Karal, F. C., Jr.(1968). Propagation of elastic waves in layered media by finite differ ence methods. *Bulletin of the Seismological Society of America, 58(1)*,367-398.

Alterman, Z & Karal Jr, FC. (1970). Propagation of elastic waves in a semi-infinite cylindrical rod using finite difference methods. *Journal of Sound and Vibration, 13*(2),115-IN1.

Andreu Alvaro Alcrudo. (2014). Evaluación de un forward modelling de ondas sísmicas. Aplicacion practica del efecto Source Ghost.

Assumpção, Marcelo & Neto, C. M. D. (2000). Sismicidade e estrutura interna da terra. *Decifrando a terra. São Paulo, Oficina de Textos,* 43-62.

Bai, C-y., Wang, X., & Wang, C-x.(2013). P-and S-wavefield simulations using both the first-and second-order separated wave equations through a high-order staggered grid finite-difference method. *Earthquake Science, 26*(2), 83-98.

Båth, M. (1966). Earthquake energy and magnitude. *Physics and Chemistry of the Earth, 7,*115-165.

Becerra Ospina, S. (2011). Propagación de ondas sísmicas y migración. *Departamento de Matemáticas*

Benito, J., Ureña, F., Gavete, L., Salete, E., & Ureña, M. (2017). Implementations with generalized finite differences of the displacements and velocity-stress formulations of seismic wave propaga tion problem. *Applied Mathematical Modelling,52,*1-14.

Contreras, X., & Aldana, M. (2012). Wave propagation: a finite difference modelling in a 3D fluid-solid configuration. *Revista tecnica de la facultad de ingenieria Universidad del Zulia, 35*(2), 179-189.

Cuminato, JA & Meneguette, MJ. (2013). *Discretizaçao de equaçoes diferenciais parciais*. Available at http://www. lcad. icmc. usp. br/ siae98.

América, Centro Regional de Sismología et al., (1997). Peligro Sismico en Latinoamerica y el Caribe: informe final; capitulo IV, América del Sur. *IPGH, México, MX*.

Erickson, J. (2014). *Making of the earth: geologic forces that shape our planet*. Infobase Publishing.

Fernandes, L, L., Cruz, J. C. R., Blanco, C. J. C. & Barp, A. R. B. (2009). Modelagem Sísmica via métodos das diferenças finitas: caso da bacia do Amazonas. *Acta Amazonica, 39*(1), 155-163.

Garcia Carvajal, O. J. et al. (2018). Contribuição ao estudo analítico de vulnerabilidade sísmica para uma configuração típica de ponte no Brasil.

Gates, A. E., & Ritchie, D. (2006). *Encyclopedia of earthquakes and volcanoes*. Infobase Publishing.

Gutenberg, B. (1945). Magnitude determination for deep-focus earthquakes. *Bulletin of the Seismologi cal Society of America, 35*(3), 117-130.

Hustedt, B., Operto, S., & Virieux, J. (2004). Mixed-grid and staggered-grid finite-difference methods for frequency-domain acoustic wave modelling. *Geophysical Journal International, 157*(3), 1269-1296.

Kious, W. J., & Tilling, R. I. (1996). *This dynamic Earth: the story of plate tectonics*. Diane. Publising.

Lisitsa, V., Tcheverda, V., & Botter, C. (2016). Combination of the discontinuous Galerkin method with finite differences for simulation of seismic wave propagation. *Journal of Computational Physics, 311*, 142-157.

Nery, G. G. (1990). Perfilagem geofísica em poço aberto. *Salvador, BA, 231p*.

Pekeris, C., Alterman, Z., Abramovici, F., & Jarosch, H. (1965). Propagation of a compressional pulse in a layered solid. *Reviews of Geophysics, 3*(1), 25-47.

Ren, Z., & Li, Z. (2019). High-order temporal and implicit spatial staggered-grid finite-difference oper ators for modelling seismic wave propagation. *Geophysical Journal International, 217*(2), 844-865.

Richards, P. G., & Aki, K. (1980). *Quantitative Seismology: Theory and Methods*. Freeman.

Rosa Filho, J. C., Soares Filho, D. M., & Mansur, W., J. (2003). Modelagem sísmica de ondas elásti cas e migração reversa no tempo em meios transversalmente isotrópicos. *8th International Congress of the Brazilian Geophysical Society,* cp-168.

Saadi, A., Machette, M. N., Haller, K, M., Dart, R. L., Bradley, L., & Souza, A. (2003). *Map and database of Quaternary faults and lineaments in Brazil*. US Geological Survey.

Santos, S. H. C., & Lima, S. (2008). S. The New Brazilian Standard for Seismic Design. *The 14th World Conference on Earthquake Engineering, Beijing, China*.

Santos, S. H. C., Lima, S. S. & Silva, F. (2010). Risco sísmico na região Nordeste do Brasil. *Revista IBRACON de Estruturas e Materiais, 3*(3), 374-389.

Silva, A., González, H., & Agudelo, W.(2009). Modelado de la Propagación de Ondas Sísmicas Basado en Algoritmo FDTD en Paralelo. *Mecánica Computacional, 28*(5), 287-293.

Sleeman, A., McConnell, B., & Gatley, S. (2004). *Understanding Earth Processes, Rocks and the Geo logical History of Ireland: A Companion to the 1: 1.000. 000 Scale Bedrock Geological Map of Ireland*. Geological Survey of Ireland.

Shedlock, K. M., Giardini, D., Grunthal, G., & Zhang, P.(2000). The GSHAP Global Seismic Hazard Map. *Seismological Research Letters, Seismological Society of America, 71*(6), 679-686.

Takenaka, H., Komatsu, M., Toyokuni, G., Nakamura, T., & Okamoto, T. (2017). Quasi-Cartesian finite-difference computation of seismic wave propagation for a three-dimensional sub-global model. *Earth, Planets and Space, 69*(1), 1-13.

USP. (2021). Website, Centro de Sismologia da Universidade de São Paulo,2021 (http://moho.iag.usp.br).

Website, Regional Center of Seismology for South America(http://www.ceresis.org/ (07/06/2020))

Vashisth, A., & Gogna, M. (1993). The effect of loose boundaries on wave propagation in a porous solid: reflection and refraction of seismic waves across a plane interface. *International journal of solids and structures, 30*(18), 2485-2499.

Virieux, J. (1986) P-SV wave propagation in heterogeneous media; velocity-stress finite-difference method. *Geophysics, 51*(4), 889-901.

Virieux, J., Etienne, V., Cruz-Atienza, V., Brossier, R., Chaljub, E., Coutant, O., Garambois, S., Mer cerat, D., Prieux, V., Operto, S., et al. (2012). Modelling seismic wave propagation for geophysical imaging.

Zhang, W., Chen, X. (2006). Traction image method for irregular free surface boundaries in finite differ ence seismic wave simulation. *Geophysical Journal International 167,*(1), 337-353.

Zhang, Z., Zhang, W., Li, H., & Chen, X. Stable discontinuous grid implementation for collocated-grid finite-difference seismic wave modelling. *Geophysical Journal International 192,*(3), 1179-1188.